BABEŞ-BOLYAI UNIVERSITY FROM CLUJ-NAPOCA
FACULTY OF CHEMISTRY AND CHEMICAL ENGINEERING
DEPARTMENT OF CHEMICAL ENGINEERING
SCIENTIFIC RESEARCH CENTER IN PHYSICAL CHEMISTRY

ABSTRACT OF DOCTORAL THESIS

RESEARCH AND DEVELOPMENT OF NANOSTRUCTURED SYSTEMS OF BIOLOGICAL AND BIOMEDICAL INTEREST

PhD CANDIDATE:
ALEXANDRA AVRAM

SCIENTIFIC ADVISOR:
UNIV. PROF. DR. MARIA TOMOAIA-COTIŞEL

CLUJ-NAPOCA
2020

BABEŞ-BOLYAI UNIVERSITY FROM CLUJ-NAPOCA

FACULTY OF CHEMISTRY AND CHEMICAL ENGINEERING

DEPARTMENT OF CHEMICAL ENGINEERING

SCIENTIFIC RESEARCH CENTER IN PHYSICAL CHEMISTRY

RESEARCH AND DEVELOPMENT OF NANOSTRUCTURED SYSTEMS OF BIOLOGICAL AND BIOMEDICAL INTEREST

ABSTRACT OF DOCTORAL THESIS

Committeee:
President:
Univ. Prof. Dr. Ion Grosu - Corresponding member of the Romanian Academy,
Director of the Doctoral School of Chemistry, Babeş-Bolyai University of Cluj-Napoca
Scientific advisor:
Univ. Prof. Dr. Maria Tomoaia-Cotişel – Director of the Center for Scientific Research in Physical Chemistry, Babeş-Bolyai University of Cluj-Napoca, Corresponding member of the Romanian Academy of Scientists
Reviewers:
Univ. Prof. Dr. Eng. George Arghir - Professor Emeritus, Technical University of Cluj-Napoca; Honorary member of the Romanian Academy of Science and Technology
Univ. Prof. Dr. Ossi Horovitz - Babeş-Bolyai University of Cluj-Napoca
Univ. Prof. Dr. Eng. Gheorghe Nechifor - Polytechnic University of Bucharest-Faculty of Applied Chemistry

Thesis defense date: September 30th 2020

THESIS TABLE OF CONTENTS:

KEYWORDS

doxorubicin, gold nanoparticles, resveratrol, doxorubicin nanocomplexes, HeLa and CaSki tumor cells, nanoceramics, stoichiometric hydroxyapatite, multisubstituted hydroxyapatite, magnesium, zinc, silicon, silver nanoparticles, nitroxoline, XRD, SEM-EDX, AFM, thermal analysis, thermal stability, forsterite, bioactivity, biocompatibility, antimicrobial activity

INTRODUCTION

Metallic nanoparticles, NPs, e.g. AuNPs and NP systems are extremely powerful tools for the selective and specific delivery of therapeutic agents, such as anti-cancer drugs such as doxorubicin, to their site of action. In general, ceramic NPs, such as unsubstituted hydroxyapatite, HAPs and multisubstituted hydroxyapatites, ms-HAPs, and magnesium silicates such as nano-forsterite, FS, are important for bone tissue engineering, as bone substitutes and biomimetic coatings on metal implants, and prostheses with biomedical applications in orthopedics and dentistry. Also, ceramic NPs can be widely used as carriers of various NPs, such as AuNPs and AgNPs, or therapeutic agents such as antibiotics, ensuring a slow delivery to their site of action. Therefore, the research and development of NPs as well as their applications are important from a scientific and industrial point of view.

The engineering of these NPs, their synthesis and physical and chemical characterization, as well as their in vitro behavior were carefully studied in this doctoral thesis under the leadership of Univ. Prof. Dr. Maria Tomoaia-Cotisel, Director of the Research Center in Physical Chemistry, CECHIF, at Babeş-Bolyai University of Cluj-Napoca, UBB. The results obtained in this doctoral thesis are part of significant achievements, achieved in the last decade in the CECHIF center at UBB.

Chapter 1 aims to investigate the effects of gold nanoparticles, obtained by reducing HAuCl4 with trans-resveratrol, Resv, alone or in combination with doxorubicin, Dox. This study presents the effects of doxorubicin, alone or in a mixture with resveratrol and AuNPs on two human cervical cancer cell lines (HeLa and CaSki). The experimental results demonstrate for the first time "in state of the art" the remarkable combined effects of doxorubicin, gold nanoparticles and resveratrol on these types of cancer cells, at very low doses of doxorubicin, a situation in which there are no side effects on healthy cells [1].

Chapter 2 reports the synthesis and physico-chemical characterization of some hydroxyapatites: Stoichiometric HAP, unsubstituted and multi-substituted with magnesium, zinc and silicon, ms-HAP-Mg-Zn-Si. Also, a study was done on the influence of heat treatment on these nanomaterials. The results indicate a very good thermal stability, which recommends these nanostructured biomaterials for various applications in bone tissue engineering [2].

Chapter 3 continues to explore the thermal stability of more complex samples of multi-substituted hydroxyapatite with essential physiological elements

such as magnesium, zinc, strontium and silicon, HAP-Mg-Zn-Sr-Si, at high temperature up to and including 1000 ºC. The objective of this study was to investigate the simultaneous effect with the four elements, Mg, Zn, Sr and Si (HAP-Mg-Zn-Sr-Si), in the HAP structure as well as the thermal behavior of the synthesized PAH biomaterials [3].

Chapter 4 presents the thermal analysis of some multi-substituted hydroxyapatite pastes (the compositions being the previous ones, HAP-Mg-Zn-Sr-Si). In this case, the water content of the pastes, an important parameter for certain applications, was determined by thermal analysis. The thermal stability of the pastes was monitored for one year; the thermal analyzes being performed after 4 months and one year after their preparation [4].

Chapter 5 addresses an in-depth study on the influence of heat treatment on multi-substituted hydroxyapatite powders in order to identify and explain the processes that can take place at different temperatures (300, 800, 1000 and 1400 ºC). These nanomaterials were analyzed by advanced physical and chemical methods: TG-DSC, RXD, FTIR coupled with Rietveld analysis of the hydroxyapatite structure investigated. An exceptional stability of the HAP structure at 1000 ºC was found, which indicates an optimal synthesis, and a rigorous pH control on the colloidal chemistry of the structuring processes of nanomaterials.

Chapter 6 focuses on the study of the antibacterial activity (ie, *Staphylococcus aureus* by Kirby-Bauer diffusion test) of ceramic samples in the form of discs, based on hydroxyapatite, previously charged with nitroxoline (antibiotic) and silver ions [5].

Chapter 7 aims to research Portland cement enriched with hydroxyapatite with endodontic applications. The main parameter followed was the setting time, a particularly important parameter in the clinical use of this nanomaterial [6].

Chapter 8 presents the study of sintering and characterization of new ceramic materials based on forsterite. Fluctuations in the characteristics of compactness (apparent density, apparent porosity) as well as shrinkage with increasing temperature (1200 and 1450 °C) are crucial parameters in the construction of bone implants. Also, cell cultures demonstrate an excellent biocompatibility of forsterite [7].

Chapter 9 evaluates the biocompatibility and bioactivity of innovative ceramic materials based on porous forsterite. In this investigation, the main objective was the development of forsterite-based ceramics with different porosities and the evaluation of its quality testing by the sintering behavior of nano forsterite powder. A detailed study was also performed for the in vitro assessment of biocompatibility in cell culture and bioactivity in simulated body fluid, SBF [8].

Chapter 10 presents nanostructured forsterite in combination with silver nanoparticles. The purpose of this chapter is to evaluate the antibacterial activity of these composites on two pathogens, *Staphylococcus aureus* 6538P (ATCC) and *Escherichia coli* 10536 (ATCC). The antimicrobial potential is particularly important in the use of forsterite for metal implant coatings with medical applications [9].

Chapter 11 is an unpublished complex study on the in vitro bacterial activity of standalone forsterite nanopowder, synthesized by two methods (sol-gel,

FSsg, and precipitation, FSpp). In-vitro antibacterial activity was investigated on a strain of *Staphylococcus aureus* 6538P (ATCC).

Chapter 12 aims to develop a fast, low-cost method for removing heavy metal ions from wastewater using a low crystallinity HAP prepared by a precipitation method. This study correlated the adsorption behavior of HAPs with low crystallinity and its efficiency in removing a wide range of various metals (Al, Cd, Co, Cr, Cu, Fe, Mn, Ni, Pb and Zn) from a mine wastewater from Roşia Montană [10].

Capitolul 13 presents the general conclusions.

Capitolul 14 is comprised of a selective reference list.

Capitolul 15 includes results from original scientific research.

Original research references:

1. Gh. Tomoaia, O. Horovitz, A. Mocanu, A. Nita, **A. Avram**, C. P. Racz, O. Soritau, M. Cenariu, M. Tomoaia-Cotisel, effects of doxorubicin mediated by gold nanoparticles and resveratrol in two human cervical tumor cell lines, Colloids and Surfaces B: Biointerfaces, 135, 726-734 (2015). **IF= 3.973**.
2. F. Goga, E.Forizs, **A. Avram**, A. Rotaru, A. Lucian, I. Petean, A. Mocanu, M. Tomoaia-Cotisel, Synthesis and thermal treatment of hydroxyapatite doped with magnesium, zinc and silicon, Revista de Chimie (Bucuresti), 68(6), 1193-1200 (2017). **IF=1.605.**
3. F. Goga, E. Forizs, G. Borodi, G. Tomoaia, **A. Avram**, R. Balint, A. Mocanu, O. Horovitz, M. Tomoaia Cotisel, Behavior of doped hydroxyapatites during the heat treatment, Revista de Chimie (Bucuresti), 68(12), 2907-2913 (2017). **IF=1.605**.
4. E. Forizs, F. Goga, **A. Avram**, A. Mocanu, I. Petean, O. Horovitz, M. Tomoaia-Cotisel, Thermal analysis of pure and multisubstituted hydroxyapatite pastes, Studia Universitatis Babes-Bolyai, Chemia 62(4), 2017, 173-180. **IF=0.275**.
5. A. Danistean, M. Gorea, **A. Avram**, S. Rapuntean, M.Aurora, G. Tomoaia, C. Garbo, O.Horovitz, M. Tomoaia-Cotisel, Antimicrobial activity of ceramic desks loaded with nitroxoline, Studia Universitatis Babes-Bolyai, Chemia, 61(3), 275-283 (2016). **IF=0.275**.
6. **A. Avram**, M. Gorea, R. Balint, L. Timis, S. Jitaru, A. Mocanu, M. Tomoaia-Cotisel, Portland cement enriched with hydroxyapatite for endodontic applications, Studia Universitatis Babes-Bolyai, Chemia, 62(4), 81-92 (2017). **IF=0.275**.
7. M. Gorea, M.-A. Naghiu, **A. Avram**, I. Petean, M. Tomoaia-Cotisel, Sintering and characterization of some new forsterite ceramics, Studia Universitatis Babes-Bolyai, Chemia, 64(2), 383-392 (2019). **IF= 0.275**.
8. M. Gorea, M.-A. Naghiu, **A. Avram**, I. Petean, A. Mocanu, M. Tomoaia-Cotisel, Novel porous forsterite ceramics. Biocompatibility and bioactivity evaluation, Revista de Chimie (Bucuresti), 71(2), 343-351 (2020). IF= **1.605**.
9. **A. Avram**, M. Gorea, S. Rapuntean, A. Mocanu, G. A. Paltinean, C. Varhelyi Jr., O. Horrovitz, M. Tomoaia-Cotisel, In-vitro antibacterial activity of novel

nanostructured composites based on forsterite and silver nanoparticles, Revista de Chimie (Bucuresti), 71(1), 13-21 (2020). IF= **1.605**.

10. **A. Avram**, T. Frentiu, O. Horovitz, A. Mocanu, F. Goga, M. Tomoaia-Cotisel, Hydroxyapatite for removal of heavy metals from wastewater, Studia Universitatis Babes-Bolyai, Chemia, 62(4), 93-104 (2017). IF=**0.275**.

Chapter 1. EFFECTS OF DOXORUBICIN MEDIATED BY GOLD NANOPARTICLES AND RESVERATROL. A STUDY IN TWO TUMOR CELL LINES - HeLa and CaSki

Gold nanoparticles (AuNPs) were prepared by green synthesis by reducing $HAuCl_4$ with trans-resveratrol in basic solution by a modified procedure. AuNPs are very stable, with an average diameter of about 20 nm. Supramolecular nano-assemblies of resveratrol-coated gold nanoparticles (AuNPs) with different doxorubicin (Dox) content were prepared by mixing the nanogold colloidal solution (Au content, 179 mg / L) with aqueous doxorubicin solution (42 mg / L doxorubicin hydrochloride) by self-assembly. The cytotoxic effects of Resv-Dox mixtures and Dox-AuNPs complexes were found in HeLa and CaSki cells for the first time.

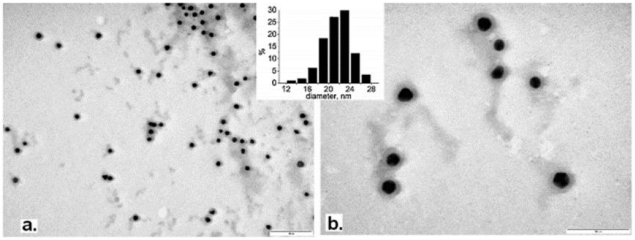

Figure 4. TEM images of the dispersion containing Dox-GNPs nanocomplex: GNPs (Au 54 mg/L), Dox (4 mg/L), and PBS; bars are 200 nm (a), respectively 100 nm (b); the histogram for size distribution is also shown.

In the TEM images (Fig. 4) of the dispersion containing the Dox-AuNPs nanocomplex, described above, the onset of nanoparticle aggregation is difficult to be observed even after two weeks. The thickness of the organic coatings also appears to remain rather unchanged, so it appears that doxorubicin molecules are trapped in the resveratrol coatings on AuNPs.

In the microscopic analysis, Resv-treated HeLa cells (Fig. 7) show a cell density that is comparable to that of untreated control cells (CTRL). The combination of resveratrol with very low doses of doxorubicin (0.1 and 0.2 g / ml, samples 2 and 3, respectively in Fig. 6a) gives a rather similar response to that for simple Dox, at the high concentration of 2.1 g / ml (Fig. 6a, sample 7). The gold nanoparticles coated with Resv (Fig. 6a, sample 4) induced only a very small effect compared to the control sample. However, like Resv-Dox mixtures, AuNPs and doxorubicin (Dox-AuNPs) nanocomplexes at very low Dox doses (Fig. 6a, samples 5 and 6) induced a response close to that of simple Dox at 2.1 µg / mL. Although, there are no statistically significant differences between the cell viability results for samples 2, 3, 5-7, they are all significantly different from the control

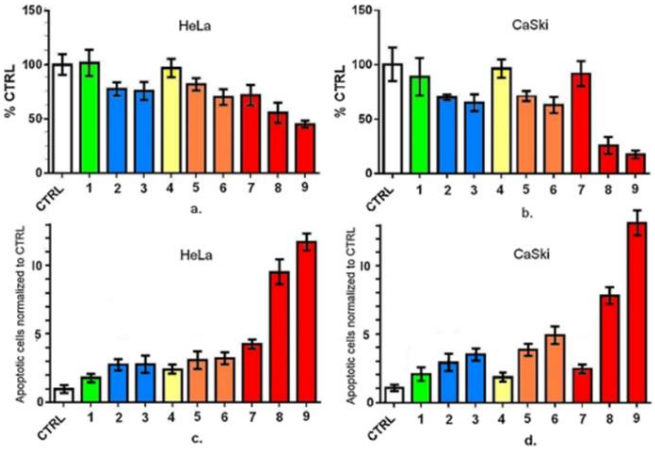

Figure 6. HeLa (a, c) and CaSki (b, d) cell response to Resv of 0.75 g/mL (sample 1), Resv-Dox mixtures: 0.5 g/mL Resv and 0.1 g/mL Dox (2), and 1 g/mL Resv and 0.2 g/mL Dox (3), GNPs of 2.7 g/mL (4), Dox-GNPs nanocomplexes, namely 0.1 g/mL Dox and 1.3 g/mL GNPs (5), and 0.2 g/mL Dox and 2.7 g/mL GNPs (6), and three free Dox concentrations: 2.10 g/mL (7), 6.25 g/mL (8) and 12.5 g/mL (9), after 24 h incubation. CTRL represents the control given by untreated cells. Cells viability was determined using MTT assay and it is given in% of CTRL (a, b). Apoptotic cells were evaluated by flow cytometry analysis; the values are normalized to the CTRL (c, d). The bar values are the mean from at least three different experiments. Error bars represent the standard deviation (± SD).

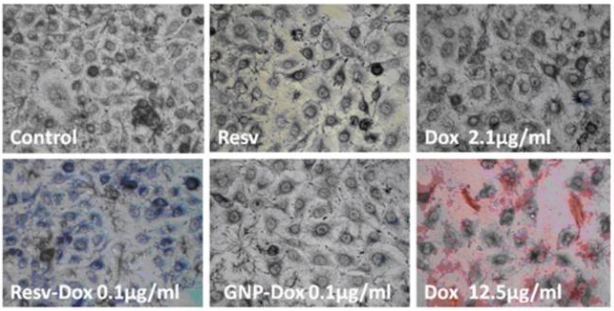

Figure 7. Phase contrast images in optical microscopy of HeLa cells treated with Resv (0.75 g/mL), Dox alone, at 2.10 and 12.5 g/mL, Resv-Dox mixture (0.5 g/mL Resv and 0.1 g/mL Dox), and Dox-GNPs nanocomplex (0.1 g/mL Dox and 1.3 g/mL GNPs). Intracellular dark purple granules indicate viable cells (Magnification× 400).

Chapter 2. SYNTHESIS AND THERMAL TREATMENT OF HYDROXIAPATITES DOPED WITH MAGNESIUM, ZINC AND SILICON

Pure nanocrystalline hydroxyapatite (Hap) and Hap doped with magnesium, zinc and silicon, namely Hap-0.25% by weight Mg: Hap01, Hap-0.25 wt% Mg-0.47 wt% Si: Hap02, Hap-1.50 wt% Mg-0.47 wt% Si: HapO3, Hap- 0.67 wt% Mg-0.2 wt% Zn-0.13 wt% Si: Hap04, were synthesized using a precipitation method from aqueous solution. Pure and doped hydroxyapatites were calcined individually at 400, 650 and 850 °C for 2 hours.

The thermal behavior of pure Hap and doped Hap powders was determined by thermogravimetric analysis (TGA) and differential thermal analysis (DTA), for temperatures ranging between 30 and 1000 °C. The analysis of the results shows a high thermal stability (up to 1000 °C) of these nanomaterials, including for triple substituted Hap with Mg, Zn and Si (Hap04).

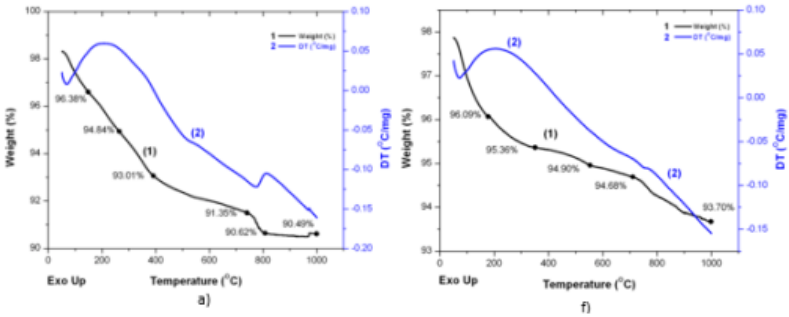

Figure 1. TG and DT curves for uncalcined Hap (Hap-nc) (Hap01, a) and Hap-0,67%Mg-0,20%Zn-0,13%Si (Hap04, f)

When heated to high temperatures up to 1000 °C, the weight loss is about 0.86% for Hap-nc, and rather close to 0.98% for Hap04. This small weight loss of approximately 1% found for these powders could be attributed to the decomposition of possible traces of $CaCO_3$ due to the synthesis of nano powder in the air and / or to the loss of lattice water. However, structural dehydroxylation of Hap and doped Hap powders cannot be ruled out at very high temperatures close to 1000 °C.

A porous aggregate structure is also revealed by Figures 3c and 3d for Hap04, calcined at 850 °C. Moreover, the SEM results are in substantial agreement with the BET measurements. Therefore, the specific surface area for Hap04 calcined at 850 °C (19 m^2 / g) is much smaller than for Hap01 (48 m^2 / g). By calcination of Hap04, the pore volume decreased from about 0.18 cm^3 / g, found at 400 °C, to about 0.02 cm^3 / g, at 850 °C and consequently, the specific surface area gradually decreased and the particle size increased. A similar situation is encountered for all samples.

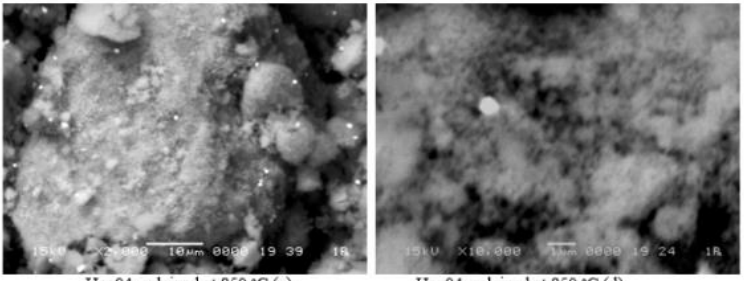

Hap04, calcined at 850 °C (c) Hap04, calcined at 850 °C (d)

Figure 3. SEM images for Hap04: $Ca_{9,69}Mg_{0,28}Zn_{0,03}(PO_4)_{5,95}(SiO_4)_{0,05}(OH)_{1,95}$ (c and d), powders calcined at 850 °C. Image scale: 10µm (c) and 1µm (d).

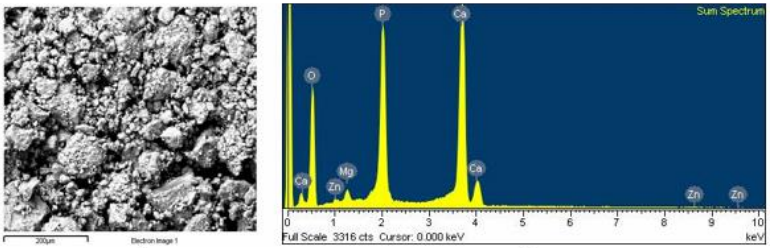

Figure 4. SEM image and EDX analysis for Hap04: $Ca_{9,69}Mg_{0,28}Zn_{0,03}(PO_4)_{5,95}(SiO_4)_{0,05}(OH)_{1,95}$ calcined at 650 °C. The quantity of Ca, P, O Mg and Zn is presented.

Elemental analysis of Hap01-Hap04 powders was determined by the SEM-EDX technique. EDX analysis showed the presence of Ca, P, Mg and O in all powders, almost corresponding to the synthesis. In addition, Si was identified in Hap02 and Hap03, while Zn was identified in Hap04 (Fig. 4).

The Si content in Hap04 was not identified as it was in a very small amount, probably below the detection limit of the EDX technique. In general, EDX analysis indicated that Mg was fairly evenly dispersed in all doped Hap powders. The EDX analysis is in accordance with the chemical composition corresponding to the synthesis.

Chapter 3. BEHAVIOR OF DOPED HYDROXIAPATITES DURING HEAT TREATMENT

Stoichiometric hydroxyapatite (HAP) and multi-doped hydroxyapatite samples, doped with essential physiological elements, such as Mg, Zn, Sr and Si, were prepared in the form of pastes with controlled humidity and powders with controlled crystallinity, which were lyophilized or lyophilized-calcined at 300 ^{o}C for 1 hour.

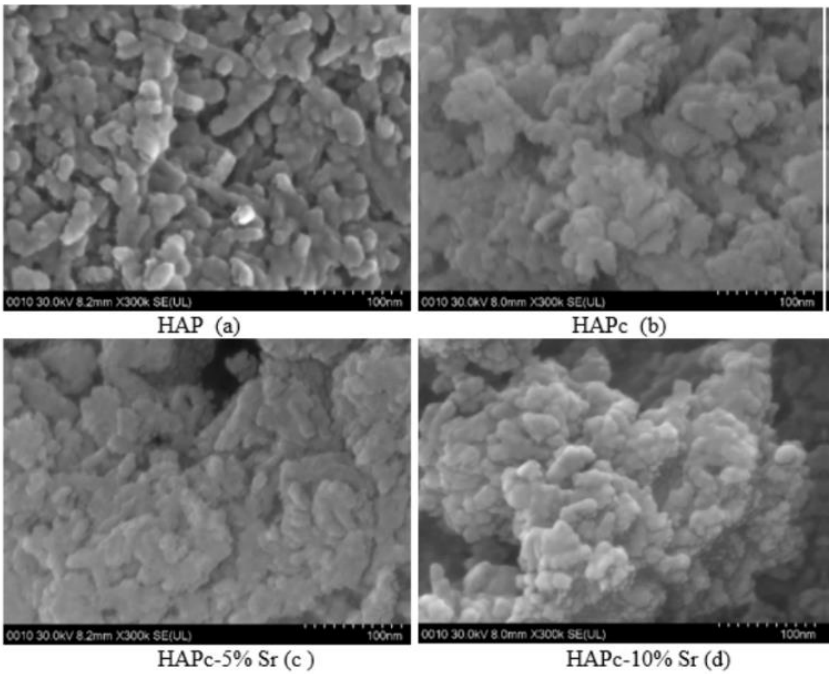

Figure 2. SEM images for powders: HAP (a), HAPc-10%Sr (d) lyophilized and calcined at 300 ^{o}C for 1 hour, 100nm scale

Figure 2 provides the morphology for calcined lyophilized HAP powders, calcined at 300 ^{o}C for 1 hour. Analyzing the SEM images, a porous structure can be observed, and the particle packaging seems significantly different from that for pure PAH morphology, depending on the composition of the biomaterial.

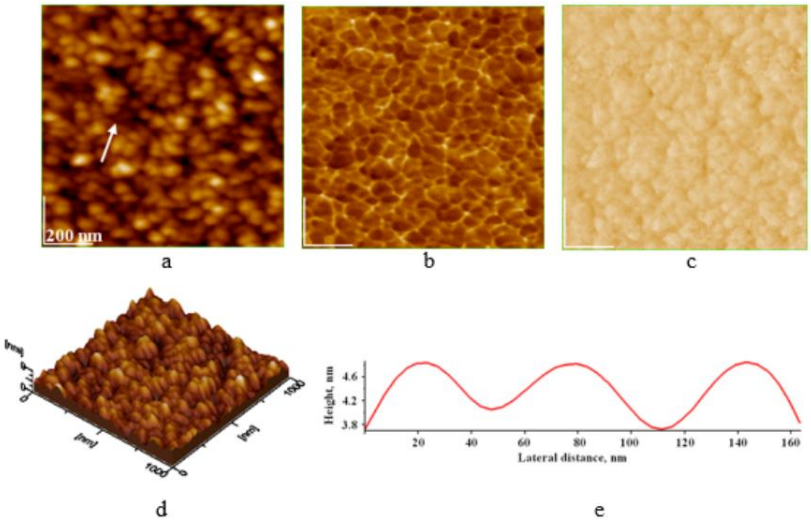

Figure 5. AFM images for HAPc-5% Sr, lyophilized powders: (a) 2D-topography, (b) phase, (c) amplitude and (d) 3Dtopography images; (e) cross section profile along the arrow in panel (a).

As an example, AFM images for uncalcined lyophilized HAPc-5% Sr powders dispersed in pure water and adsorbed as a self-assembled layer on glass are shown in Figure 5. As observed in the 2D topography (Fig. 5a), the phase image (fig. 5b), amplitude image (fig. 5c), 3D topography (fig. 5d) and in the cross section profile (fig. 5e).

The particle shape is almost spherical with an average diameter of 39 ± 2 nm. AFM images also confirmed an average particle size for all calcined lyophilised powders, as follows 45 ± 3 nm for HAP, 40 ± 2 nm for HAPc, 37 ± 3 nm for HAPc-5% Sr and 35 ± 2 nm for HAPc-10% Sr.

In particular, AFM images indicated that nanoparticles of HAP powders, uncalcined lyophilized or calcined lyophilized, consist of particles of almost identical size in very good agreement with the crystallite size determined in the X-diffraction data.

Chapter 4. THERMAL ANALYSIS OF PURE AND MULTISUBSTITUTED HYDROXYAPATITE PASTES

The thermal stability of pure and multisubstituted hydroxyapatite (HAP) pastes, doped with magnesium, silicon, strontium and zinc, synthesized using an aqueous precipitation method, was investigated.

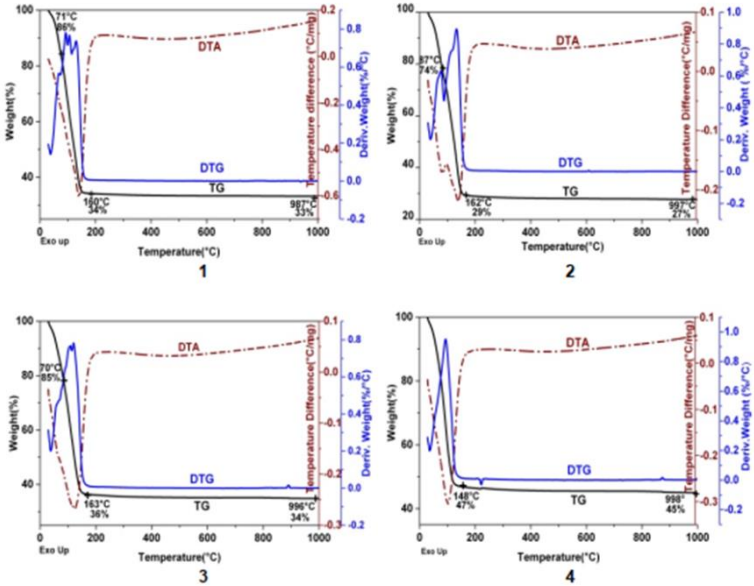

Figure 1. Thermal curves of the four pastes: 1) pure HAP (sample 1); 2) HAP 1.5%Mg, 0.2%Si, 0.2%Zn (sample 2); 3) HAP 1.5%Mg, 0.2%Si, 0.2%Zn, 5%Sr (sample 3); 4) HAP 1.5%Mg, 0.2%Si, 0.2%Zn, 10%Sr (sample 4), after 4 months.

The thermal curves (TG, DTA) of pure and doped HAP pastes have the same shape in the range of 30-1000 °C. After 4 months, no significant differences in thermal behavior were observed. The only difference is in the moisture content of the sample. Thermogravimetric monitoring of weight loss shows that the weight of all samples decreases continuously with increasing temperature. The highest weight loss occurs in the range of 30-200 ° C and can be attributed to the very high water content of the pastes, because water molecules surround hydroxyapatite particles. The corresponding DTA data indicate an endothermic transformation for all samples at approximately 160 °C.

Chapter 5. INFLUENCE OF SUBSTITUTION ELEMENTS AND THERMAL TREATMENT ON THE STRUCTURE OF MULTISUBSTITUTED HYDROXIAPATITES

This study focuses on the synthesis and characterization of unsubstituted and / or substituted hydroxyapatites (HAPs) with Mg, Zn, Si and Sr. All HAP nanomaterials were synthesized using a wet precipitation method. 4 series of HAPs (HAP1, HAP2, HAP3 and HAP4) were synthesized and characterized, each uncalcined lyophilized (lnc) and calcined lyophilized (lc), at 4 chosen calcination temperatures, 300, 800, 1000, 1400 ^{o}C, resulting in a total of 20 compounds with HAP structure.

Thermal stability was monitored for each nanomaterial, i.e. uncalcined lyophilized HAP (lnc) and calcined lyophilized (lc) one hour each. The thermal stability of unsubstituted hydroxyapatite was also determined in accordance with the requirements of ISO 13779-3: 2008, mainly at 1000 ^{o}C, for calcination for 15 h.

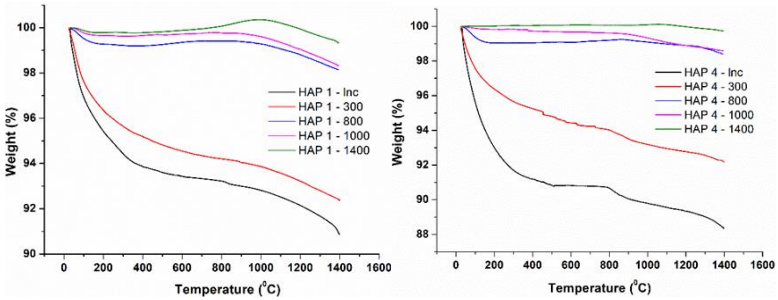

A D

Figura 1. TG curves for HAP 1 and HAP 4, both uncalcined lyophilized (lnc), and thermally treated at the 4 experimental temperatures (300, 800, 1000, 1400 ^{o}C): A) HAP 1; D) HAP 4

It can be seen that all uncalcined lyophilized hydroxyapatites suffer a higher mass loss than the heat-treated ones, the mass loss decreasing with increasing temperature. For uncalcined samples, the total weight loss varies between 9.13% and 12.44%, the lowest value being in the unsubstituted HAP sample, and increases in the substituted one. The thermal behavior of the calcined samples at 300 ^{o}C is very similar to the uncalcined ones, the differences being the lower values of the total mass losses due to the elimination of physical water during calcination. In samples calcined at high temperatures, 800, 1000 and 1400 ^{o}C, the mass losses are significantly reduced, because all the decomposition processes present up to 800 ^{o}C took place during the calcination. The values of the total mass loss in these samples are below 2%, in some

cases on small temperature ranges there is even a slight increase in mass (0.2%) due to rehydration during the thermal analysis.

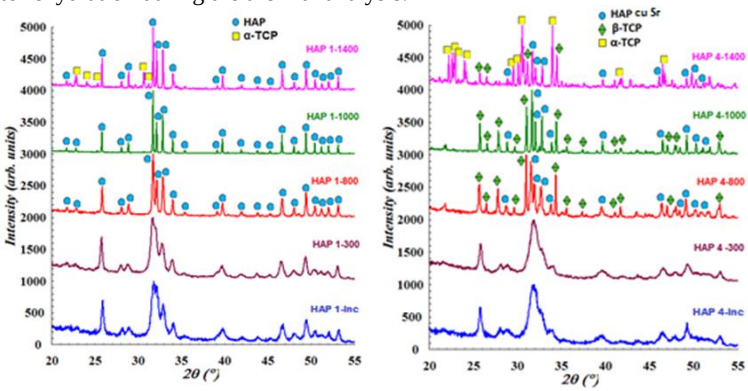

A D

Figure 3. XRD diffractograms for samples HAP1 (A, HAP), and HAP4 (D, HAP-1,5%Mg- 0,2%Si-0,2%Zn- 10%Sr), lyophilized uncalcined (lnc) and lyophilized calcined, at selected temperatured, (300 °C, 800 °C, 1000 °C si 1400 °C), for 1 hour. HAP-Sr is the compound: $(Ca_{8.98}Sr_{1.02})(PO_4)_6(OH)_2$;

It can be seen that HAP1 (Figure 3A) contains hydroxyapatite as a single phase up to and including 1000 °C (PDF 72-1243) for one hour of calcination. For the HAP4 sample (Figure 3D) the appearance of beta tricalcium phosphate (PDF 70-2065) at 800 °C can be observed. An increase in the calcination temperature to 1400 °C highlights the presence of a minor secondary phase, alpha- tricalcium phosphate (α-TCP, $Ca_3(PO4)_2$, PDF 70-0364).

Table 3. Crystallite sizes, crystallinity degree for HAP1 and HAP4

No.	Sample	Crystallite size (nm)	Crystallinity degree (%)
1	HAP1-lnc	39	52.5
2	HAP1-300	43	55.3
3	HAP1-800	63	99.2
4	HAP1-1000	128	100.0
5	HAP1-1400	144	100.0
16	HAP4-lnc	32	38.2
17	HAP4-300	36	40.1
18	HAP4-800	56	98.6
19	HAP4-1000	89	99.8
20	HAP4-1400	97	100.0

As shown in Table 3, the crystallite sizes are the smallest (i.e., 32-39 nm) for all lyophilized and uncalcined samples. The size of the crystallites increases strongly with the increase in calcination temperature.

Chapter 6. ANTIMICROBIAL ACTIVITY OF CERAMIC DISKS LOADED WITH SILVER IONS AND NITROXOLINE

This chapter discusses the use of porous discs of stoichiometric hydroxyapatite (HAP) loaded with silver ions and nitroxoline (5-nitro-8-hydroxyquinoline, NHQ) in vitro against pathogens such as *Staphylococcus aureus*. Two synthesized HAP powders are used, namely HAP1 calcined at 450 ºC and HAP2 further calcined at 850 ºC.

Table 1. Characteristics of the ceramic disks

Ceramic discs	Sample No.	Apparent density ρ_a (%)	Water absorption a_m (%)	Apparent porosity P_a (%)
HAP1	1	1.24	38.27	47.67
	2	1.36	34.41	47.01
	3	1.46	37.31	54.73
HAP2	1	1.57	29.44	46.39
	2	1.31	36.70	48.12
	3	1.21	36.63	44.56

The compactness characteristics of sintered ceramic discs were determined using Archimedes' method. The apparent density, ρa, water absorption, am and the apparent porosity, Pa were determined (Table 1). The apparent porosity of the ceramic discs is high. This property allows various solutions to penetrate the porous disks and provides an optimal choice for the adsorption on the disk surface of the components in the solutions. Consequently, active silver ions and NHQ biomolecules, impregnated in HAP discs, can be released into the microbial environment.

Figure 4 shows representative images of agar plates with *Staphylococcus aureus* cultures of after incubation at 37 °C for 24 hours, with ceramic discs (Figure 4a) and with the initial solutions in which the discs had been immersed (Figure 4b) . The diameters of the inhibition zones, in mm, are shown in Table 2. The control discs, samples 1 and 6 (HAP1, HAP2, in pure water) do not produce any inhibition zone. The greatest effect is observed for the discs loaded with NHQ, sample 4 (HAP1) and sample 8 (HAP2) (Figure 4a) and for their corresponding NHQ solutions, which remained after the discs were removed (approximately 24 hours after preparation) for antimicrobial evaluation (Figure 4b). The antimicrobial effect of the HAP1 disc impregnated with NHQ (sample 4) was very strong (> 30 mm) and comparable to that of sample 8, HAP2 / NHQ. This is clear evidence that NHQ adsorbed and incorporated into ceramic discs has a strong effect on *S. aureus*.

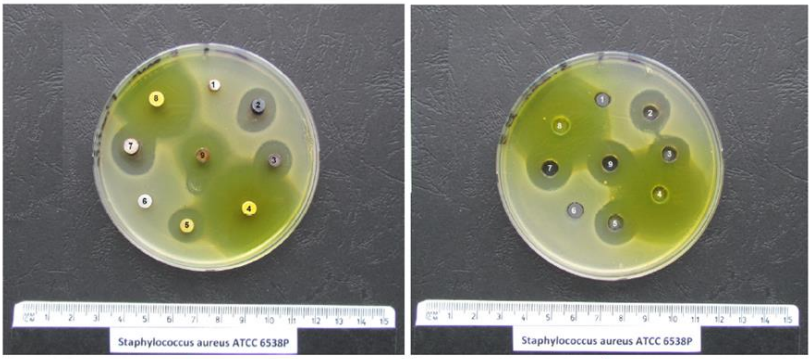

a. b.

Figura 4. Inhibition zones for *Staphylococcus aureus* in presence of ceramic disks loaded with antimicrobial solutions (a), or in presence of antimicrobial solutions in wells (b). Samples are numbered as follows: 1 for HAP1/water and 6: HAP2/water, each as control; 2 and 3: HAP1/$AgNO_3$; 7: HAP2 /$AgNO_3$; 4: HAP1/NHQ; 8: HAP2/NHQ; 5: HAP2/NHQ + $AgNO_3$; 9: HAP1/NHQ + $AgNO_3$

Table 2. Inhibition zones for samples presented in Figure 4; The lables are the same as in Figure 4

Sample	Inhibition zones (mm)								
	1	***2***	***3***	***4***	***5***	***6***	***7***	***8***	***9***
Disks	-	15	15	>30	14	-	17	>30	18
Solutions	-	18	18	>30	17	-	18	>30	18

The antimicrobial effect of NHQ-loaded ceramic discs is also comparable to that of NHQ solutions (samples 4 and 8, in Figure 4b) which show that *S. aureus* is very sensitive in vitro to NHQ. The discs charged with Ag^+ ions (Figure 4a) and their corresponding $AgNO_3$ solutions (Figure 4b), namely samples 2, 3 and 7, also show distinct areas of inhibition. The antimicrobial effect of the HAP1 disc loaded with Ag^+ (samples 2 and 3, Figure 4a) is smaller than that corresponding to the Ag^+ solutions (Figure 4b). The cause could be the interaction of Ag^+ with the surface of the ceramic nanoparticles inside the disk leading to a slowed supply of Ag^+. However, the area of inhibition is almost the same (Table 2) for the HAP2 disc loaded with Ag^+ (sample 7, Figure 4a) and for Ag^+ in solution (sample 7, Figure 4b). This shows that these features of HAP disks are also important.

The antimicrobial effect (Table 2) for the HAP1 disc (sample 9) previously immersed in the initial NHQ solution for 30 min, is greater than that of the HAP2 disc immersed for 15 min (sample 5), both immersed, after removal from NHQ , in 5 ml 10^{-2} M solution of $AgNO_3$ each.

Chapter 7. PORTLAND CEMENT ENRICHED WITH HYDROXYAPATITE FOR ENDODONTIC APPLICATIONS

This paper focuses on endodontic cement obtained from Portland cement enriched with two types of hydroxyapatite, simple and doped with 5% Zn. Hydroxyapatites were synthesized using a wet precipitation method and were investigated by X-ray diffraction, FTIR, TEM and AFM. From a structural point of view, both hydroxyapatites were obtained in a single crystalline phase, which contains particles in the nanometric range, as shown by XRD, TEM and AFM analyzes. Several experimental compositions of commercial Portland cement mixed with hydroxyapatite were prepared.

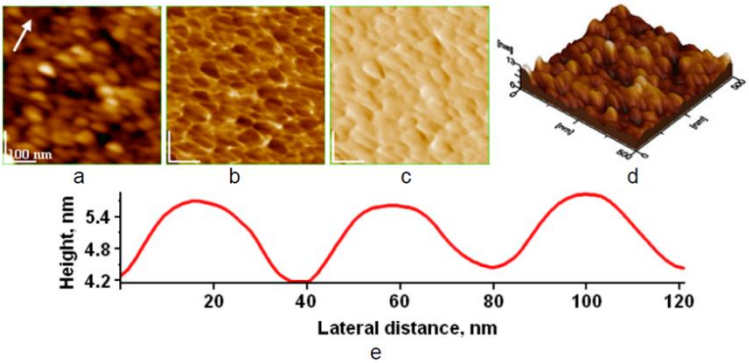

Figure 5. AFM images of HAP-5%Zn particles adsorbed on glass for 10 sec from aqueous dispersion: 2D topography (a), phase (b), amplitude (c), 3D- topography (d) and cross section profile (e) along the arrow in image (a); scanned area of 0.5 μm x 0.5 μm; average nanoparticle size of 27 nm

Most particles are elongated, with a length of about 40/20 nm for Zn-doped hydroxyapatite.

In the experiments, stoichiometric, uncalcined hydroxyapatite and Zn-doped hydroxyapatite were mixed together with Portland cement. The compositions of the endodontic cement samples are shown in Table 2. Sample S0 is composed only of Portland cement and is the standard sample. Cements S1, S2, S3 and S4 contain different amounts of stoichiometric hydroxyapatite, while endodontic cements S5, S6 and S7 contain different amounts of Zn-doped hydroxyapatite.

The experimental data regarding the setting times of the studied endodontic cements, which contain a water of consistency of 87 ml, at temperatures of 22 °C and 37 °C, are presented in table 4.

Table 2. The studied compositions of endodontic cements

Material (%) / Sample	Stoichiometric HAP	Zn doped HAP	Portland cement
S0	-	-	100
S1	1	-	99
S2	2	-	98
S3	3	-	97
S4	5	-	95
S5	-	1	99
S6	-	2	98
S7	-	3	97

The setting times for all experimental samples, including the standard, S0, decrease with the increase in temperature temperature from 22 °C to 37 °C, the normal temperature of the human body. No difference can be observed by adding 1 and 2 wt% of uncalcined hydroxyapatite (samples S1 and S2). Sample S3, which contains 3 wt% hydroxyapatite, shows a more pronounced decrease in setting time at both working temperatures. By increasing the hydroxyapatite content by up to 5 wt%, as seen in sample S4, a halving of the endodontic cement setting time can be observed.

A progressive decrease in the setting time for all samples containing Zn-doped hydroxyapatite, namely S5, S6 and S7, can also be observed. Sample S7, which contains 3 wt% of Zn-doped hydroxyapatite, shows a behavior similar to sample S3, which contains 3 wt% of stoichiometric hydroxyapatite. The two types of hydroxyapatite show comparable results in reducing the setting time of endodontic cement.

Table 4. Setting time of Portland cement and studied endodontic cements

Sample	Consistency water (ml)	Setting time (min)	
		at 22 ° C	at 37 ° C
S0	87	85	70
S1		70	60
S2		70	60
S3		55	45
S4		45	35
S5		70	65
S6		65	60
S7		55	45

Chapter 8. SINTERING AND CHARACTERIZATION OF NEW FORSTERITE CERAMICS

This study shows the sintering of new forsterite (FC) ceramics using nano forsterite powder, obtained by a sol-gel method. The forsterite ceramic was sintered between 1200 and 1450 °C. Forsterite ceramics (FC) have undergone some changes in their structural characteristics, such as apparent porosity, apparent density, and linear shrinkage depending on the sintering temperatures, 1200, 1300, 1400 and 1450 °C used in the production process (FC (1200)), FC (1300), FC (1400) and FC (1450)).

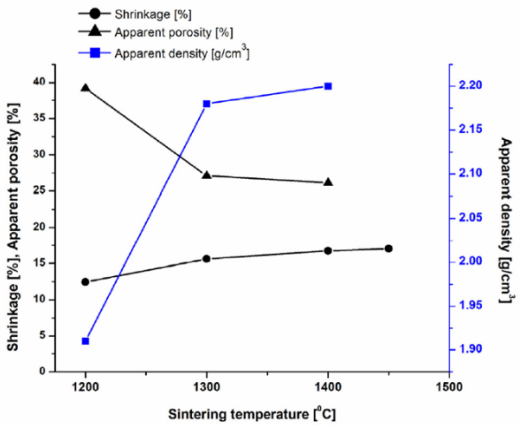

Figure 1. Apparent density, apparent porosity and linear shrinkage determined for forsterite ceramics in function of sintering temperature.

As shown in Figure 1, the linear shrinkage of the sintered forsterite ceramics displayed a steady increase from 12.46±0.16% to 17.03±0.15%, with an increase in sintering temperature from 1200 to 1450 °C. Apparent density increased from 1.91 ±0.02 to 2.33±0.01 (g/cm^3), while the corresponding porosity decreased from 39.15±0.16 to 25.05±0.14 %. Statistical analysis evaluated with GraphPad Prism program showed that increasing the sintering temperature induced an increase in linear shrinkage. Statistically significant differences ($p < 0.05$) evaluated by one-way ANOVA and Bonferroni's multiple comparison test were observed between forsterite ceramics sintered at 1200 °C versus all the others forsterite ceramics sintered at chosen temperatures. Strong differences were also identified between forsterite ceramics sintered at 1300 °C versus both ceramics sintered at 1400 °C and 1450 °C. No significant differences were found between ceramics sintered at 1400 °C and 1450 °C. The order among forsterite ceramics (FC) is: FC(1200) <FC(1300)< FC(1400)≈ FC(1450).

Chapter 9. NOVEL POROUS FORSTERITE CERAMICS. BIOCOMPATIBILITY AND BIOACTIVITY EVALUATION

The study aims to evaluate the biocompatibility and bioactivity of new porous forsteritic (FC) ceramics produced from high-purity nano-forsterite powder, synthesized by an original sol-gel method, which was then pressed into pellets using a polyvinyl alcohol solution as a binding agent. The raw pellets were then sintered at 1200 °C, 1300 °C, 1400 °C and 1450 °C. The four obtained forsterite ceramics, FC-1200, FC-1300, FC-1400 and FC-1450, were completely characterized by density, porosity and shrinkage measurements.

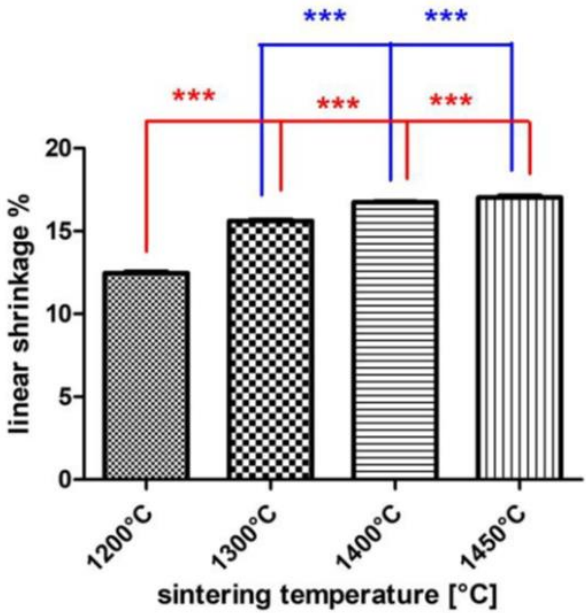

Figure 1. Linear shrinkage (LS) of forsterite ceramics (FCs) versus sintering temperature. Error bars stand for standard deviation (SD); the tips of error bars just touch the average values, indicating high data quality with an excellent reproducibility. Data are given as mean ± SD. Statistically significant differences for $p<0.001$ are (***) marked

As indicated in Figure 1, the statistical analysis showed a significant difference between linear shrinkage (LS) for FC- 1200 vs FC-1300, and FC-1400, and FC-1450 (red stars), as well as for FC-1300 vs FC-1400, and FC-1450 (blue stars), for $p<0.001$; while LS for FC-1400 vs LS for FC-1450 were not statistically different, $p>0.001$. The following order FC-1200< FC-1300<FC-1400, was found for $p<0.001$. So, the highest LS value (%) of 16.73 ± 0.13 was found for FC-1400. These data,

shown in Figure 1, revealed that FC-1400 is apparently the best regarding the compactness of particles in the fosterite ceramics potentially of interest for bone repair defects.

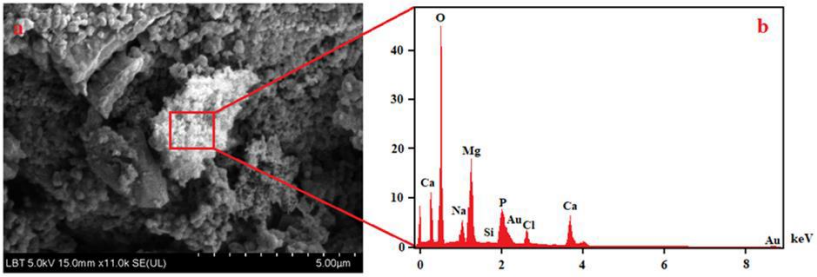

Figure 5. SEM image (a) and EDS spectrum (b) for forsterite ceramic, FC-1400, after 3 months of immersion in SBF

The SEM image for surface morphology and EDS spectrum obtained on forsteritic ceramics, FC-1400 sintered at 1400 °C, immersed in SBF for 3 months, is shown in Figure 5. In the SEM image, Figure 5, newly formed hydroxyapatite crystals are highlighted on the surface of forsteritic ceramics, FC-1400. The EDS spectrum in the area containing hydroxyapatite crystals shows the presence of calcium and phosphorus together with silicon and magnesium, belonging to FC. Thus, it is demonstrated that by maintaining the FCs samples in SBF, hydroxyapatite crystallites are initiated and grow on porous forsteritic ceramics.

Figure 6 shows the results of the MTT test for forsteritic ceramics, FC-1200, for different time intervals in HFL culture. Cell viability was assessed with the MTT test and showed a gradual increase in cell proliferation on FC-1200 scaffolds, with statistically significant differences between 3 versus 7 days and between 3 versus 14 days, in fibroblast culture ($p < 0.001$), but without a statistically significant difference between 7 and 14 days in cell culture, $p > 0.001$.

Therefore, the cell density on FC-1200 scaffolds increased with incubation time to 7 days without a significant increase between 7 and 14 days after seeding. The results indicate that FC-1200 scaffolds can promote cell adhesion, proliferation and growth and therefore have excellent biocompatibility.

In addition, the 14-day test in culture shows that cell proliferation is only slightly increased compared to the level reached at 7 days and without statistical significance. Therefore, the highest level for cell viability and proliferation was reached at 7 days for FC-1200 in HFL culture, when the surface of the scaffolds was completely covered with adherent cells.

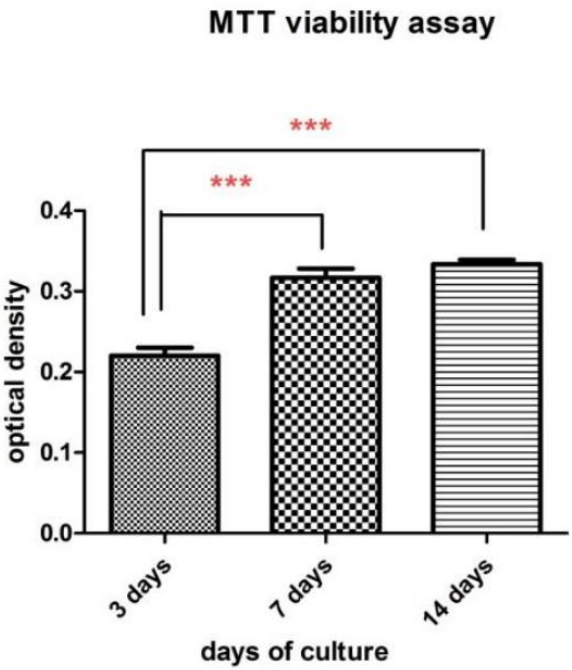

Figure 6. Cell viability and proliferation rate, given as optical density (OD) units, of HFL cells cultivated on FC-1200 scaffolds for 3, 7 and 14 days by using MTT test. Error bars stand for standard deviation (SD). Statistical analysis of OD (average values) indicates significant differences for $p<0.001$ and are (***) marked

Chapter 10. IN_VITRO ANTIBACTERIAL ACTIVITY OF NOVEL NANOSTRUCTURED COMPOSITES BASED ON FORSTERITE AND SILVER NANOPARTICLES

This study was performed to evaluate the antimicrobial activity of two nanostructured forsterite powders, both in the absence and presence of silver nanoparticles (AgNPs). The two forsterite powders (FS) were prepared by advanced methods of synthesis, sol-gel (FSsg) and precipitation (FSpp). The preparation of colloidal AgNPs was performed using the precursors, $AgNO_3$, trisodium citrate and tannic acid, ensuring the formation and stabilization of AgNPs.

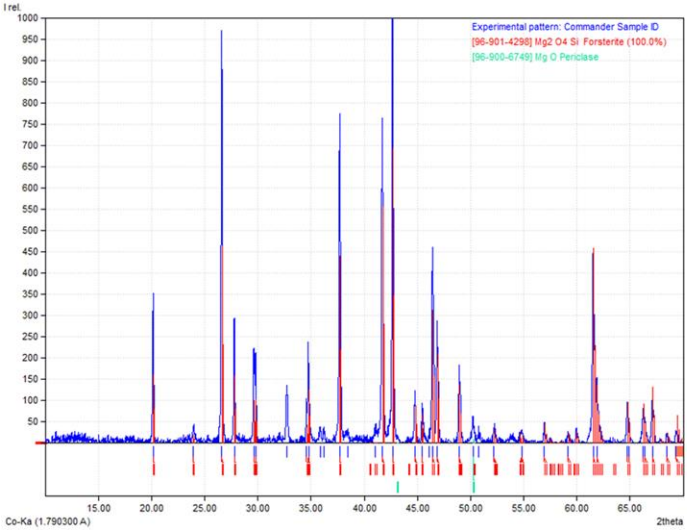

Figura 1. X-ray diffraction for FSsg powder

The XRD diffraction spectrum is shown in Figure 1 for the FSsg powder. The XRD spectrum shows a well crystallized phase with narrow, very well defined peaks. Moreover, Figure 1 shows forsterite as a single phase with only traces of magnesium oxide (MgO).

The forsterite obtained by the sol-gel method was investigated in the presence of AgNPs both in neutral medium (pH-7) and in alkaline medium (pH-12), related to the FSsg content, having a constant amount of 0.25 mM AgNPs. Aspects of the mode of action of the FSsg product on the tested strains are shown in Table 1 and Figures 9a and 9b. Testing of the antibacterial effect of the obtained forsterite, FSsg and FSpp, variants with AgNPs and variants without AgNPs, namely forsterite in pure water, as well as in neutral pH and in alkaline pH media, was performed by the agar diffusion method against strains. *S. aureus* and *E. coli*.

Table 1. FSsg content of samples prepared in two media of pH 7 and distinctly pH 12 at the same content in AgNPs (0.25 mM), and the diameter of zones of inhibition at 24 h, tested strains: *S. aureus* și *E. coli*.

Tested strain	**Composite characteristics**			
	AgNPs in aqueous medium of pH-7, versus FSsg content		AgNPs in aqueous medium, of pH-12, versus FSsg content	
	Diameter of inhibition areas (mm) for the four wells			
	1 (4 mg FSsg/ mL)	**3** (8 mg FSsg/ mL)	**2** (4 mg FSsg/ mL)	**4** (8 mg FSsg/ mL)
S. aureus 6538P ATCC	10	9	9	8
E. coli 10536 ATCC	0	0	0	0

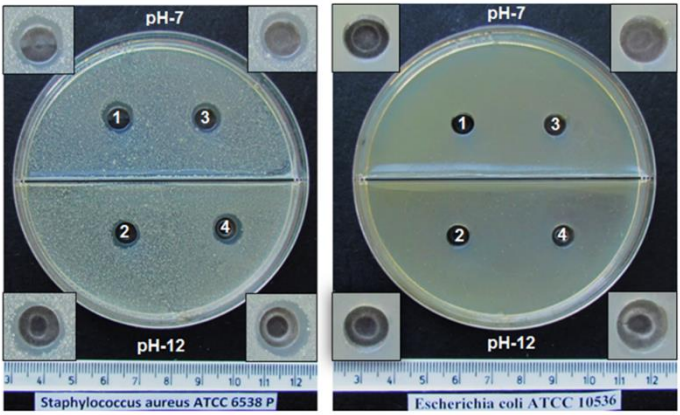

Figura 9. Inhibition zones for Staphylococcus aureus 6538P ATCC (a) and lack of inhibition for Escherichia coli 10536 ATCC (b), versus pH value and FSsg content. Wells are numbered according to their FSsg content and pH value, (see Table 1); well 1: 4 mg of FSsg/mL, pH 7; well 2: 4 mg FSsg/mL, pH 12; well 3: 8 mg FSsg/mL, pH 7; well 4: 8 mg FSsg/mL, pH 12; each sample has the same content 0.25 mM AgNPs. Insets: magnified images for each well

From the analysis of the data listed in Table 1 and Figures 9a and 9b, it can be seen that the FSsg product had only an inhibitory effect on the *S. aureus* strain. The zones of inhibition were between 8 and 10 mm and were not influenced by pH or the amount of FSsg (at 4 mg / ml and 8 mg / ml). We also mention that the inhibition areas did not change their dimensions after storing the plates for another 3 days at room temperature (in humid rooms). No inhibitory effect was found on the *E. coli* strain.

Chapter 11. IN-VITRO ANTIBACTERIAL ACTIVITY OF FORSTERITE NANOPOWDER

Forsterite nanopowder (FS) was prepared by two methods, namely sol-gel (FSsg) and precipitation (FSpp). To characterize both FSsg and FSpp, the TG-DSC, XRD, TEM and AFM methods were used. The in vitro antibacterial activity was investigated on an *S. aureus* 6538P strain (ATCC).

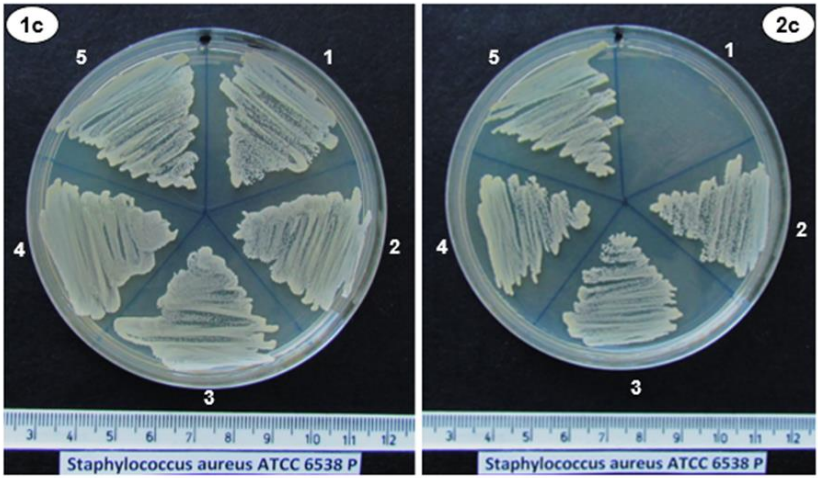

a b

Figure 13. Antimicrobial testing for samples FSsg 1c (a) and FSpp 2c (b) against *Staphylococcus aureus*: 1 = 10 mg; 2 = 5 mg; 3 = 2,5 mg; 4 = 1,25 mg; 5 = control (without forsterite)

In sample 1c (FSsg) no inhibitory effect was observed at any dilution, with the development of colonies in all the corresponding triangles of the Petri dish in which the inoculations were made (positions 1, 2, 3 and 4), including the triangle corresponding to the control tube (position 5) (figure 13 a).

In sample 2c (FSpp), an inhibitory effect was found in tube 1 (containing 10 mg of solid forsterite + 1 ml of nutrient broth), noting the absence of colonies in the corresponding triangle (position 1). At the other dilutions, namely 5 mg, 2.5 mg and 1.25 mg, no inhibitory effect was observed, with the development of colonies in all corresponding triangles (positions 2, 3 and 4), including the triangle corresponding to the control tube (position 5) (figure 13 b).

Identical results were obtained after testing with samples 1a and 2a, thus demonstrating that FSpp induces an inhibitory effect at the first dilution (10 mg FSpp + 1 ml broth) and has no inhibitory effect at lower dilutions. The plates shown in Figure 12 were kept under observation for another 5 days (in damp microrooms), without any changes compared to the initial appearance.

From the primary tubes with FSgs (10 mg + 1 ml broth) and FSpp (10 mg + 1 ml broth), which were seeded in the above-mentioned plates, maintained at laboratory temperature (48 hours), seeding was performed by striations on a Petri dish with Muller Hinton agar, divided into two halves: the left side 1a and 1c (FSsg) and the right side 2a and 2c (FSpp).

The plates were introduced at 37 ^{o}C for 24 hours. The interpretation found a lack of inhibitory effect on FSgs 1a and FSgs 1c (colony development) and an inhibitory effect on FSpp 2a and FSpp 2c (lack of colony development, the environment remains sterile) (Figure 14 a and b). The results obtained in the two tests with products 1a and 2a, respectively 1c and 2c were identical.

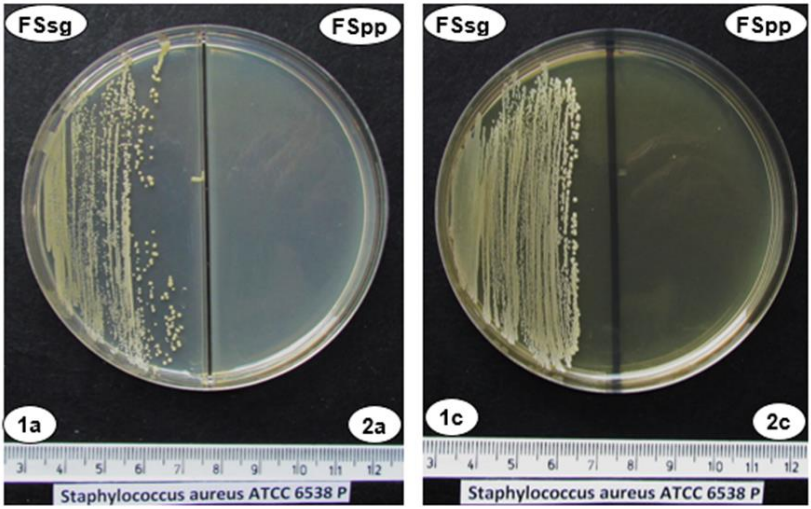

Figure 14. Inhibitory effect of FSsg si FSpp asupra *Staphylococcus aureus*, 1a, 1c (FSsg): lack of inhibitory effect (colony development); 2a, 2c (FSpp): existing inhibitory effect (lack of colony developmet)

Chapter 12. HYDROXYAPATITE FOR THE REMOVAL OF HEAVY METALS FROM WASTEWATER

Hydroxyapatite powder (HAP) of low crystallinity and a fairly large specific surface area was synthesized by a precipitation method. HAP has been used to remove metals (Al, Cd, Co, Cr, Cu, Fe, Mn, Ni, Pb and Zn) from mining wastewater. Metal contents in the initial and treated samples were quantified by inductively coupled plasma atomic emission spectrometry and high-resolution continuum source atomic absorption spectrometry. By the use of HAP, an efficient removal of all metals was ensured. The increase of Ca2+ ions content in the treated water suggests an ion exchange mechanism.

Table 1. Removal of metals from wastewater using nanometric HAP powder (results are given as mean ± standard deviation)

Metal	Initial content c_0, mg/L	Final content c_e, mg/L	Removal degree, %[a]	Limit values for wastewater, mg/L
Al	313 ± 37	1.9 ± 0.6	99.39 ± 0.24	5 (STAS 9411-83)
Cd	0.21 ± 0.07	0.068 ± 0.043	67.6 ± 1.2	0.2 (SR EN ISO 5961:2002)
Co	1.1 ± 0.6	0.15 ± 0.07	86.4 ± 1.1	1 (SR ISO 8288:2001)
Cr	0.046 ± 0.024	0.009 ± 0.006	80.4 ± 1.1	1 (SR EN 1233:2003)
Cu		0.014 ± 0.011	98.6 ± 1.4	0.1 (SR ISO 8288:2001)
Fe	1.0 ± 0.7	0.9 ± 0.6	99.02 ± 0.20	5 (SR ISO 6332-96)
Mn	92 ± 9	0.81 ± 0.48	99.57 ± 0.05	1 (SR ISO 6333-96)
Ni	189.7 ± 4.3	0.16 ± 0.09	66.0 ± 1.0	0.5 (SR ISO 8288:2001)
Pb	0.47 ± 0.22	0.066 ± 0.045	58.8 ± 1.0	0.2 (STAS 8637-79)
Zn	0.16 ± 0.07	0.18 ± 0.08	98.75 ± 0.13	0.5 (SR ISO 8288:2001)
	14.4 ± 0.9			

[a] the degree of distance and its confidence interval were calculated by a common standard difference and deviation

the removal degree, R(%) was calculated as:

$$R(\%) = 100\frac{c_0 - c_e}{c_0} \quad (2)$$

where c0 is the element' content (mg/L) in the initial mine wastewater sample, while ce is its final content at equilibrium, after adsorption for 120 min on HAP. The initial and final content and the calculated removal degree for each metal are given in Table 1, along with the standard errors from determinations on 3 parallel samples. In the same table the limit values for the metal content admissible in wastewater discharged in natural waters are indicated.

All metal ions are removed to final values below the values admitted in standards for wastewaters. The removal degree is near to 100% for metals existent in higher amounts in the wastewater, and lower (60-80%) for those present initially only in very low concentration (even under the admitted limit value – Table 1). Probably, their sorption on the surface of HAP nanoparticles is

limited by the simultaneous sorption of ions existent in high excess in the wastewater. The confidence intervals are wide due to the existence of some metals (Cu, Cr, Pb, Ni) near the quantification limit of analytical methods. However, an efficient removal of these metals below the values of admitted levels in wastewater in the presence of those in high concentrations can also be observed.

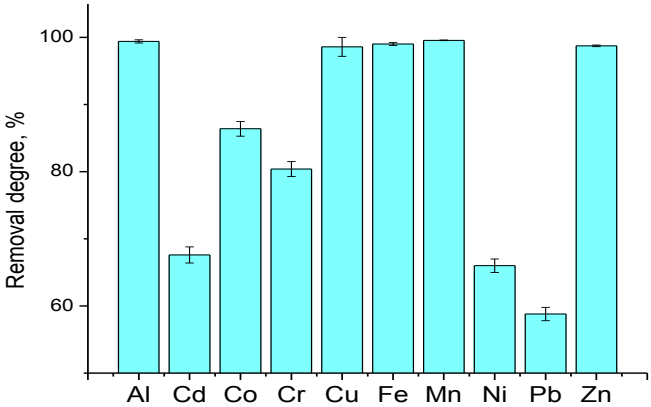

Figure 5. The removal degree of metals from mine wastewater on HAP with low crystalinity

The concentration of Mn2+ ions in mine wastewater was measured at different time points. The Mn uptake, x, from the contaminated solution on the HAP, was calculated in mg Mn/g HAP for each moment by the formula:

$$x = \frac{(c_0 - c_t)V}{m} \qquad (3)$$

where co is the initial Mn^{2+} content, ct is the content at time t (mg/L), V is the volume of solution (0.1 L), and *m* is the mass of HAP (10 g). These values are introduced in table 2.

Table2. Mn^{2+} adsorption on HAP nanoparticles

Contact time, t, min.	Mn^{2+} content t,c, mg/L	x, mg/g	x_e-x, mg/g	ln(x_e-x)	t/x, min.g/mg	$t^{1/2}$, $min^{1/2}$
0	189.7	0	1.8905	0.6368	0	0
1	146.6	0.4310	1.4595	0.3781	2.3202	1
2	108.3	0.8140	1.0765	0.0737	2.4570	1.4142
15	3.925	1.8578	0.0327	-3.4195	8.0743	3.8730
30	1.951	1.8775	0.0130	-4.3436	15.9788	5.4772
60	1.156	1.8855	0.0050	-5.2903	31.8228	7.7460
120	0.811	1.8889	0.0016	-6.4440	63.5294	10.954
240	0.726	1.8897	0.0008	-7.2089	127.002	15.492
300	0.707	1.8899	0.0006	-7.5056	158.74	17.321
600	0.659	1.8904	0.0001	-9.5670	317.39	24.495
960	0.652	1.8905	0		507.81	30.984

Chapter 13. GENERAL CONCLUSIONS

1. In vitro viability testing of two human cervical tumor cell lines (HeLa and CaSki) with different behavior in terms of chemosensitivity to Dox, led to a reversal of chemoresistance for cells treated with new gold nanocomplexes with doxorubicin stabilized with Resv, at a much lower concentration of Dox, compared to the same degree of cellular response to Dox alone, at higher doses.

2. Stoichiometric hydroxyapatite powders were prepared - HAP and multisubstituted - HAP-0.25% mg, HAP-0.25% Mg-0.47% Si, HAP 1.5% Mg-0.47% Si, HAP- 0.67% Mg-0.2% Zn-0.13% Si, HAP-1.5% Mg-0.2% Si-0.2% Zn, HAP-1.5% Mg-0.2% Si-0.2% Zn-5% Sr, HAP-1.5% Mg-0.2% Si-0.2% Zn-10% Sr. Thermal stability studies performed by thermal analysis (TG-DSC-DTA) have demonstrated excellent thermal stability of all HAP compositions. For example, stoichiometric HAp is stable up to 1000 ^{o}C in accordance with ISO 13779-3: 2008.

3. Stoichiometric hydroxyapatite pastes were prepared - HAP, and multisubstituted - HAP-1.5% Mg-0.2% Si-0.2% Zn, HAP-1.5% Mg-0.2% Si-0, 2% Zn-5% Sr, HAP-1.5% Mg-0.2% Si-0.2% Zn-10% Sr. The results of the thermal analysis confirm a high thermal stability of pure and multi-doped hydroxyapatite pastes, up to 1000 °C, even after aging for 1 year from their preparation. The thermal behavior of pure and doped hydroxyapatite pastes over time shows that this depends mainly on the loss of physically and chemically adsorbed water.

4. Porous ceramic disks made of hydroxyapatite, HAP, loaded with silver ions and nitroxoline (5-nitro-8-hydroxyquinoline, NHQ) were prepared and used in vitro against pathogens such as *Staphylococcus aureus*. The results demonstrate for the first time the ability of NHQ and Ag^{+} to diffuse from ceramic discs and exert their antimicrobial effect.

5. Experimental compositions of endodontic cement obtained from Portland cement enriched with two types of hydroxyapatite were prepared, simple and doped with 5% Zn (1, 2, 3, 5 wt%). The setting time was tested at 22 ^{o}C and 37 ^{o}C. The setting time for both sets of samples, with the addition of stoichiometric, uncalcined hydroxyapatite (S1-S4) and Zn-doped hydroxyapatite (S5-S7) decreased exponentially at both working temperatures.

6. Forsterite-based ceramics (Mg_2SiO_4) sintered at 1200, 1300, 1400 and 1450 ^{o}C were obtained (marked FC (1200), FC (1300), FC (1400) and FC (1450)). The apparent porosity of the four forsterite ceramics gradually decreased with increasing sintering temperature from about 39% for 1200 °C to 25% for 1450 °C. FC (1400) developed a fairly high hardness of about 3 GPa.

7. The linear shrinkage values (%) for forsterite ceramics show an almost linear increase, with significant differences between all CF in the temperature range from 1200 to 1400 ºC, from 12.46 ± 0.16% to 16.73 ± 0.13%. There is a nonlinear dependence of the relative density on the sintering temperatures. The relative density increased from 59.1 ± 0.8% to 68.2 ± 0.6%, with a significant difference between FC-1200 and FC-1300 and FC-1400, for $p < 0.05$, but without a significant difference between FC-1300 compared to FC-1400, $p > 0.05$. Total porosity decreased from 40.83 ± 0.11% to 31.77 ± 0.08%, with significant differences between all CFs.

8. The fosterite ceramic FC (1200) revealed an excellent biocompatibility in HFL culture, assessed by the FDA test. By increasing the maintenance time of forsterite ceramic scaffolds, FC (1200) in the culture medium, from 1 to 3 and 7 days, the number of living cells also increased. Cell density on FC-1200 scaffolds increased with incubation time up to 7 days without a significant increase between 7 and 14 days after seeding.

9. Nanostructured composites based on forsterite (obtained by sol-gel, FSsg, and precipitation, FSpp) and silver nanoparticles were obtained. Their antibacterial activity on *Staphylococcus aureus (S. aureus)* and *Escherichia coli (E. coli)* was studied. The inhibitory effect of the synthesized forsterite, FSsg and FSpp, in the variants with AgNPs was found only on the *S. aureus* strain, the inhibition areas being between 8 and 10 mm and more intensely expressed in the FSpp product. The difference between FSsg and FSpp can be related to the size of the nanoparticles in these nanomaterials.

10. The inhibitory effect of FSsg-AgNPs and FSpp-AgNPs was not significantly influenced by neutral pH and alkaline pH or by the amount of fosterite / mL (i.e. 4 mg / mL and 8 mg / mL, respectively) present in different samples / products. Thus, an optimal amount of forsterite of 4 mg / ml was recorded in this study.

11. Forsterite, FSsg or FSpp, used only in pure water, as well as in neutral medium (pH-7) and alkaline medium (pH-12), in the absence of AgNPs, had no inhibitory effect on the bacterial strains tested.

12. The antibacterial inhibitory effect of stand-alone forsterite obtained by sol-gel (FSsg) and precipitation (FSpp) was tested on a strain of *Staphylococcus aureus (S. aureus).* Testing of FSgs and FSpp products, using the nutrient broth dilution method, showed that an inhibitory effect on *S. aureus* strain was found only in the FSpp product, at a dilution of 10 mg / 1 ml and not at lower dilutions (5 mg / ml, 2.5 mg / ml and 1.25 mg / ml). Inoculation on Petri dishes with Mueller Hinton agar confirmed that the FSsg product has no inhibitory effect (development of colonies in the culture plate), and the FSpp product has a bactericidal inhibitory effect (lack of development of colonies in the culture plate). Seeding in nutrient broth tubes also confirmed that

the FSsg product has no inhibitory effect (turbidity in the culture tube), and the FSpp product has an inhibitory effect (the broth remained clear, being sterile).

13. In relation to different contact times, 5, 10, 15, 30 and 60 minutes, it was found that both FSsg and FSpp products do not have inhibitory capacity, developing colonies in the control Petri dish. Extending the contact time to 24 hours, it was found that the FSgs product has no inhibitory capacity, while the FSpp product produced inhibition, the effect being bactericidal.

14. Hydroxyapatite - HAP has been used to remove metals (Al, Cd, Co, Cr, Cu, Fe, Mn, Ni, Pb and Zn) from mining wastewater. The metal content of the initial and treated samples was quantified by inductively coupled plasma atomic emission spectrometry and high resolution continuous source atomic absorption spectrometry. By using HAPs, an efficient removal of all metals was ensured. The increase in Ca^{2+} ion content in the treated water suggests an ion exchange mechanism.

15. The structure of HAP by Rietveld refinement is given. Hydroxyapatite crystallizes in the hexagonal crystallographic system, has the spatial group P63 / m and the following network parameters: a = b = 9.4166 Å; c = 6.8745 Å; cell volume = 527.91 $Å^3$. Substitution with other cations takes place primarily in the Ca2 position and then in the Ca1 position, depending on the concentration of the substituent ion.

Chapter 14. SELECTIVE REFERENCES

1. B. Duncan, C. Kim, V.M. Rotello, Gold nanoparticle platforms as drug and biomacromolecule delivery systems, Journal of Controlled Release,148(1), 122–127 (2010).
2. S. Rana, A. Bajaj, R. Mout, V.M. Rotello, Monolayer coated gold nanoparticles for delivery applications, Advanced Drug Delivery Reviews, 64(2), 200–216 (2012).
3. J. Turkevich, P.C. Stevenson, J.A. Hillier, A study of the nucleation and growth processes in the synthesis of colloidal gold, Discussions of the Faraday Society, 11, 55–75 (1951).
4. M. Brust, M. Walker, D. Bethell, R. Schiffrin, D.J. Whyman, Synthesis of thiol-derivatised gold nanoparticles in a two-phase Liquid–Liquid system, Journal of the Chemical Society, Chemical Communications, 7, 801–802 (1994).
5. R.D. Pasca, A. Mocanu, S.D. Cobzac, I. Petean, O. Horovitz, M. Tomoaia-Cotisel, Biogenic syntheses of gold nanoparticles using plant extracts, Particulate Science and Technology, 32(2), 131–137 (2014).
6. O. Horovitz, G. Tomoaia, A. Mocanu, T. Yupsanis, M. Tomoaia-Cotisel, Protein binding to gold colloids, Gold Bulletin, 40, 213–218 (2007).
7. F. Wang, Y.C. Wang, S. Dou, M.H. Xiong, J. Sun, T.M. Wang, Doxorubicin-tethered responsive gold nanoparticles facilitate intracellular drug delivery for overcoming multidrug resistance in cancer cells, ACS Nano 5(5), 3679–3692 (2011).
8. A. Agarwal, M.A. Mackey, M.A. El-Sayed, R.V. Bellamkonda, Remote triggered release of doxorubicin in tumors by synergistic application of thermosensitive liposomes and gold nanorods, ACS Nano 5(6), 4919–4926 (2011).
9. J. Nam, W.G. La, S. Hwang, Y.S. Ha, N. Park, N. Won, S. Jung, S.H. Bhang, Y.J. Ma, Y.M. Cho, M. Jin, J. Han, J.Y. Shin, E.K. Wang, S.G. Kim, S.H. Cho, J. Yoo, B.S. Kim, pH responsive assembly of gold nanoparticles and “spatiotemporally concerted” drug release for synergistic cancer therapy, ACS Nano 7(4), 3388–3402, (2013).
10. M.F. Tang, L. Lei, S.R. Guo, W.L. Huang, Recent progress in nanotechnology for cancer therapy, Chinese journal of Cancer, 29(9), 775–780,(2010).
11. B.L. Liu, X. Zhang, W. Zhang, H.N. Zhen, New enlightenment of French Paradox: resveratrol's potential for cancer chemoprevention and anti-cancer therapy, Cancer Biology & Therapy, 6(12), 1833–1836 (2007).
12. A. Güder, H. Korkmaz, H. Gökce, Y.B. Alpaslan, G. Alpaslan, Isolation, characterization, spectroscopic properties and quantum chemical computations of an important phytoalexin resveratrol as antioxidant component from Vitis labrusca L. and their chemical compositions Spectrochimica acta. Part A, Molecular and Biomolecular Spectroscopy, 133 378–395 (2014).
13. M. Athar, J.H. Back, X. Tang, K.H. Kim, L. Kopelovich, D.R. Bickers, A.L. Kim,

Resveratrol: a review of pre-clinical studies for human cancer prevention, Toxicology and Applied Pharmacology, 224(3), 274–283 (2007).
14. E.L. Wightman, J.L. Reay, C.F. Haskell, G. Williamson, T.P. Dew, D.O. Kennedy, Effects of resveratrol alone or in combination with piperine on cerebral blood flow parameters and cognitive performance in human subjects: a randomised, double-blind, placebo-controlled, cross-over investigation, The British Journal of Nutrition, 112(2), 203–213 (2014).
15. R. Pangeni, J.K. Sahni, J. Ali, S. Sharma, S. Baboota, Resveratrol: review on therapeutic potential and recent advances in drug delivery, Expert opinion on Drug Delivery, 11(8), 1285–1298 (2014).
16. L. Zhang, F. Yang, J.Y. Cai, P.H. Yang, Z.H. Liang, In-situ detection of resveratrol inhibition effect on epidermal growth factor receptor of living MCF-7 cells by Atomic Force Microscopy, Biosensors & Bioelectronics, 56, 271–277 (2014).
17. J.K. Aluyen, Q.N. Ton, T. Tran, A.E. Yang, H.B. Gottlieb, R.A. Bellanger, Resveratrol: potential as anticancer agent, Journal of Dietary Supplements, 9, 45–56 (2012).
18. F. Huang, X.N. Wu, J. Chen, W.X. Wang, Z.F. Lu, Resveratrol reverses multidrug resistance in human breast cancer doxorubicin-resistant cells, Experimental and Therapeutic Medicine, 7(60, 1611–1616 (2014).
19. K.S. Stakleff, T. Sloan, D. Blanco, S. Marcanthony, A. Booth, T.D. Bishayee, Resveratrol exerts differential effects in vitro and in vivo against ovarian cancer cells, Asian Pacific Journal of Cancer Prevention,13(4), 1333–1340 (2012).
20. C. de Martel, J. Ferlay, S. Franceschi, J. Vignat, F. Bray, M. Forman, D. Plummer, Global burden of cancers attributable to infections in 2008: a review and synthetic analysis, The Lancet Oncology, 13(6), 607–615 (2012).
21. D. Subramanya, P.D. Grivas, HPV and cervical cancer: updates on an established relationship, Postgraduate Medicine, 120(4), 7–13 (2008).
22. M. Schiffman, P.E. Castle, J. Jeronimo, S. Rodriguez, A.C. Wacholder, Human papillomavirus and cervical cancer, Lancet, 370(9590), 890–907 (2007).
23. L.A. Padilla, B.S. Leung, L.F. Carson, Evidence of an association between human papillomavirus and impaired chemotherapy-induced apoptosis in cervical cancer cells, Gynecologic Oncology, 85(1), 59–66 (2002).
24. D. Pectasides, K. Kamposioras, E. Papaxoinis, G. Pectasides, D. Pectasides, K. Kamposioras, E. Papaxoinis, G. Pectasides, Cancer Treat. Rev. 34 (2008) 603–613, Cancer Treatment Reviews, 34(7), 603–613 (2008).
25. J.R. Chen, Y.C. Yang, T.C. Chen, J.C. Lai, S.J. Chang, C.L. Chang, K.L. Wang, Salvage chemotherapy in recurrent cervical cancer with biweekly pegylated liposomal Doxorubicin (lipo-dox), Taiwanese Journal of Obstetrics & Gynecology, 47(3), 322–326 (2008).
26. S.E. Al-Harthi, O.M. Alarabi, W.S. Ramadan, M.N. Alaama, H.M. Al-Kreathy, Z.A. Damanhouri, L.M. Khan, A.M.M. Osman, Amelioration of doxorubicin-induced cardiotoxicity by resveratrol, Moleculer Medicine Reports, 10, 1455–1460 (2014).

27. A.M.M. Osman, H.M. Bayoumi, S.E. Al-Harthi, Z.A. Damanhouri, M.F. ElShal, Modulation of doxorubicin cytotoxicity by resveratrol in a human breast cancer cell line, Cancer Cell International. 12(1), 47 (2012).
28. T.H. Kim, Y.J. Shin, A.J. Won, B.M. Lee, W.S. Choi, J.H. Jung, H.Y. Chung, H.S.
Kim, Resveratrol enhances chemosensitivity of doxorubicin in multidrug-resistant human breast cancer cells via increased cellular influx of doxorubicin, Biochimica et Biophysica Acta, 1840(1), 615–625 (2014).
29. M. Jeyaraj, R. Arun, G. Sathishkumar, D. MubarakAli, M. Rajesh, G. Sivanandhan, G. Kapildev, M. Manickavasagam, A. Thajuddin, N. Ganapathi, An evidence on G2/M arrest, DNA damage and caspase mediated apoptotic effect of biosynthesized gold nanoparticles on human cervical carcinoma cells (HeLa), Materials research Bulletin, 52, 15–24 (2014).
30. A. Mocanu, I. Cernica, Gh. Tomoaia, L.D. Bobos, O. Horovitz, M. Tomoaia-Cotisel, Self-assembly characteristics of gold nanoparticles in the presence of cysteine, Colloids Surfaces A: Physicochemical Engineering. Aspects 338(1), 93–101(2009).
31. Gh. Tomoaia, P.T. Frangopol, O. Horovitz, L.D. Bobos, M. Mocanu, M. Tomoaia-Cotisel, The effects of arginine on gold nanoparticles in colloidal solutions and in thin films, Journal of Nanoscience and nanotechnology, 11(9), 7762–7770 (2011).
32. J. Hansen, P. Bross, A cellular viability assay to monitor drug toxicity, Methods in Molecular Biology – Protein misfolding and cellular stress in disease and aging, 648, 303–311 (2010).
33. R.J. Hunter, Zeta Potential in Colloid Science: Principles and applications, Ed: R. H. Ottewill, R. L. Rowell, Academic Press, London, 1-398 (1981).
34. F. Billes, I. Mohammed-Ziegler, E. Mikosch, H. Tyihák, Vibrational spectroscopy of resveratrol, Spectrochimica acta. Part A, Molecular and Biomolecular Spectroscopy, 68(3), 669–679 (2006).
35. J.M. López-Nicolás, F. Garcia-Carmona, Aggregation state and pKa values of (E)-resveratrol as determined by fluorescence spectroscopy and UV-visible absorption, Journal of Agricultural and Food Chemistry, 56 ,7600–7605 (2008).
36. R.J. Sturgeon, S.G. Schulman, Electronic absorption spectra and protolytic equilibria of doxorubicin: direct spectrophotometric determination of microconstants, Journal of Pharmaceutical Sciences, 66(7), 958–961 (1977).
37. S.P. Garcia-Zepeda, E. Garcia-Villa, J. Diaz-Chávez, R. Hernández-Pando, P. Gariglio, Resveratrol induces cell death in cervical cancer cells through apoptosis and autophagy, European Journal of Cancer Prevention, 22(6), 577–584 (2013).
38. P. Zhang, H. Li, B. Yang, F. Yang, L.L. Zhang, Q.Y. Kong, X.Y. Chen, M.L. Wu, J. Liu, Biological significance and therapeutic implication of resveratrol-inhibited Wnt, Notch and STAT3 signaling in cervical cancer cells, Genes & Cancer, 5(5-6), 154–164 (2014).

39. K. Song, P. Xu, Y. Meng, F. Geng, J. Li, Z. Li, J. Xing, J. Chen, B. Kong, Smart gold nanoparticles enhance killing effect on cancer cells, International Journal of Oncology, 42, 597–608 (2013).
40. D. Goren, A.T. Horowitz, D. Tzemach, M. Tarshish, S. Zalipsky, A. Gabizon, Nuclear delivery of doxorubicin via folate-targeted liposomes with bypass of multidrug-resistance efflux pump, Clinical Cancer Research, 6(5), 1949–1957 (2000).
41. A. Bigi, E. Boanini, C. Capuccini , M. Gazzano , Strontium-substituted hydroxyapatite nanocrystals, Inorganica Chimica Acta, 360, 1009-1016 (2007).
42. F. Goga, E. Forizs, G. Borodi, G. Tomoaia, A. Avram, R. Balint, A. Mocanu, O. Horovitz, M. Tomoaia Cotisel, Behavior of doped hydroxyapatites during the heat treatment, Revista de Chimie.(Bucharest), 68(12), 2907-2913 (2017).
43. D. Laurencin, N. Almora-Barrios, N.H. De Leeuw, C. Gervais, C. Bonhomme, F. Mauri, W. Chrzanowski, J.C. Knowlws, R.J. Newport, A. Wong, Z. Gan, M.E. Smith, Magnesium incorporation into hydroxyapatite, Biomaterials, 32(7), 1826-1837 (2011).
44. Gh. Tomoaia, A. Mocanu, I. Vida-Simiti, N. Jumate, L. D. Bobos, O. Soritau, M. Tomoaia-Cotisel, Silicon effect on the composition and structure of the composition and structure of nanocalcium phosphates In vitro biocompatibility to human osteoblasts, Materials Science and engineering C, 37, 37-47 (2014).
45. Z.Y. Qiu, I.S. Noh, S.M. Zhang, Silicate-doped hydroxyapatite and its promotive effect on bone mineralization Frontiers of Material Science, 7(1), 40-50 (2013).
46. E. Boanini, M. Gazzano, A. Bigi, Ionic substitutions in calcium phosphates synthesized at low temperature, Acta Biomaterialia, 6(6), 1882-1894 (2010).
47. J.H. Shepherd, D.V. Shepherd, S.M. Best, Substituted hydroxyapatites for bone repair, Journal of Materials Science: Materials in Medicine, 23(10), 2335-2347 (2012).
48. C.F. Marques, A. Lemos, S.I. Vieira, O.A.B. Da Cruz e Silva, A. Bettencourt, J.M.F. Ferreira, Antibiotic-loaded Sr-doped porous calcium phosphate granules as multifunctional bone grafts, Ceramics International, 42, 2706-2716 (2016).
49. B. Wopenka, J.D. Pasteris, A mineralogical perspective on the apatite in bone, Materials Science and Engineering C, 25, 131-143 (2005).
50. M. Veiderma M., Studies on the termochemistry and thermal processing of apatite, Procedings of the Estonian Academy of Sciences. Chemistry, 49, 631-672 (2000).
51. K.A. Gross, C.C. Berndt, Biomedical application of apatites, Phosphates: geochemical, geobiological and material importance, Reviews in Mineralogy and Geochemistry, 48, 427-454 (2000).
52. A.A. Chaudry, J. Goodal, M. Vickers, J.K. Cockroft, I. Rehman, J. Campbell Knowles, J.A. Darr, Synthesis and characterisation of magnesium

substituted calcium phosphate bioceramic nanoparticles made via continuous hydrothermal flow synthesis, Journal of Materials Chemistry, 18, 5900-5908 (2008).
53. G. Furtos, M. Tomoaia-Cotisel, C. Garbo, M. Senila, N. Jumate, I. Vida-Simiti, C. Prejmerean, New Composite Bone Cement Based on Hydroxyapatite and Nanosilver, Particulate Science and Technology, 31(4), 392-398 (2013).
54. A. Mocanu, G. Furtos, S. Rapuntean, O. Horovitz, C. Flore, C. Garbo, A. Danisteanu, Gh. Rapuntean, C. Prejmerean, M. Tomoaia-Cotisel, Synthesis characterization and antimicrobial effects of composites based on multi-substituted hydroxyapatite and silver nanoparticles, Applied Surface Science, 298, 225-235 (2014).
55. Gh. Tomoaia, O. Soritau, M. Tomoaia-Cotisel, L. B. Pop, A. Pop, A. Mocanu, O. Horovitz, L. D. Bobos, Scaffolds made of nanostructured phosphates, collagen and chitosan for cell culture, Powder Technology, 238, 99-107 (2013).
56. A. Mocanu, R. Balint, C. Garbo, L. Timis, I. Petean, O. Horovitz, M. Tomoaia-Cotisel, Low Crystallinity Nanohydroxyapatite Prepared at Room Temperature, Studia UBB Chemia, 62(2), 95-103 (2017).
57. A. Danistean, M. Gorea, A. Avram, S. Rapuntean, Gh. Tomoaia, A. Mocanu, C. Garbo, O. Horovitz, M. Tomoaia-Cotisel, Antimicrobial activity of ceramic disks loaded with silver ions and nitroxoline, Stud UBB Chemia, 61(3), Tom I, 275-283 (2016).
58. P.T. Frangopol, A. Mocanu, V. Almasan, C. Garbo, R. Balint, G. Borodi, I. Bratu, O. Horovitz, M. Tomoaia-Cotisel, Synthesis and structural characterization of strontium substituted hydroxyapatites, Revue Roumine de Chimie, 61(4-5), 337-344 (2016).
59. C. Prejmerean, M. Tomoaia-Cotisel, E. Vasile, G. Furtos, L. B. Pop, M. Moldovan, C. Sarosi, I. Petean, Characterisation of surface organisation and morphology of some new experimental dental resin-based composites, International Journal of Nano and Biomaterials, 3(4), 344-359 (2011).
60. F. Goga, E. Forizs, A. Avram, A. Rotaru, A. Lucian, I. Petean, A. Mocanu, M. Tomoaia-Cotisel, Synthesis and thermal treatment of hydroxyapatite doped with magnesium, zinc and silicon, Revista de Chimie (Bucharest), 68(6), 1193-1200 (2017).
61. C. Garbo, M. Sindilaru, A. Carlea, Gh. Tomoaia, V. Almasan, I. Petean, A. Mocanu, O. Horovitz, M. Tomoaia-Cotisel, Synthesis and structural characterization of novel porous zinc substituted nanohydroxyapatite powders, Particulate Science and Technology, 35(1), 29-37 (2017).
62. D. Oltean-Dan, G. B. Dogaru, M. Tomoaia-Cotisel, D. Apostu, A. Mester, H. R. C. Benea, M. G. Paiusan, E. M. Jianu, A. Mocanu, R. Balint, C. O. Popa, C. Berce, G. I. Bodizs, A. M. Toader, Gh. Tomoaia, Enhancement of bone consolidation using highfrequency pulsed electromagnetic short-waves and titanium implants coated with biomimetic composite embedded into PLA matrix: in vivo evaluation, International Journal of nanomedicine, 14, 5799-5816 (2019).

63. S. Rapuntean, P. T. Frangopol, I. Hodisan, Gh. Tomoaia, D. Oltean-Dan, A. Mocanu, C. Prejmerean, O. Soritau, L. Z. Racz, M. Tomoaia-Cotisel, In vitro Response of Human Osteoblasts Cultured on Strontium Substituted Hydroxyapatites, Revista de Chimie (Bucharest), 69(12), 3537-3544 (2018).
64. A. Avram, M. Gorea, R. Balint, L. Timis, S. Jitaru, A. Mocanu, M, Tomoaia-Cotisel, Portland Cement Enriched With Hydroxyapatite For Endodontic Applications, Studia UBB Chemia, 62(4), 81-92 (2017).
65. A. Avram, T. Frentiu, O. Horovitz, A. Mocanu, F. Goga, M. Tomoaia-Cotisel, Hydroxyapatite For Removal Of Heavy Metals From Wastewater, Studia UBB, Chemia, 62(4), 93-104 (2017).
66. E. Forizs, F. Goga, A. Avram, A. Mocanu, I. Petean, O. Horovitz, M. Tomoaia-Cotisel, Thermal Analysis Of Pure And Multisubstituted Hydroxyapatite Pastes, Studia UBB Chemia, 62(4), 173-180 (2017).
67. C. Garbo, J. Locs, M. D'Este, G. Demazeau, A. Mocanu, C. Roman, O. Horovitz, M. Tomoaia-Cotisel, Advanced Mg, Zn, Sr, Si Multi-Substituted Hydroxyapatites for Bone Regeneration, International Journal of nanomedicine, 15, 1037-1058 (2020).
68. K. Tonsuaadu, K.A. Gross, L. Pluduma, M. Viederma, A review on the thermal stability of calcium apatites, Journal of Thermal Analysis and Calorimetry, 110, 647-659 (2012).
69. C.-J. Liao, F.-H. Lin, K.-S. Chen, J.-S. Sun, Thermal decomposition and reconstituition of hydroxyapatite in air atmosphere, Biomaterials, 20, 1807-1813 (1999).

70. Z. Zyman, I. Ivanov, D. Rochmisttrov, V. Glushko, N. Tkachenko, S. Kijio, Sintering peculiarities for hydroxyapatite with different degrees of crystalinity, Journal of Biomedical Materials Research, 54, 256-263 (2001).
71. S. Kannan, I.A.F. Lemos, J.H.G. Rocha, J.M.F. Ferreira, Synthesis and characterization of magnesium substituted biphasis mixtures of controlled hydroxyapatite/β-tricalcium phosphate ratios, Journal of Solid State Chemistry, 178, 3190-3196 (2005).
72. R. Enderle, F. Gotz-Neunhoeffer, M. Gobbels, F.A. Muller, P. Greil, Influence of magnesium doping on the phase transformation temperature of β-TCP ceramics examined by Rietveld refinement, Biomaterials, 26, 3379-3384 (2005).
73. J. Terra, E. Rodrigues Dourado, J.-G. Eon, D.E. Ellis, G. Gonzales, A. Malta Rossi, The structure of strontium-doped hydroxyapatite: an experimental and theoretical study, RCS Physical Chemistry Chemical Physics, 11, 568-577 (2009).
74. M.D. O'Donell, Y. Fredholm, A. de Rouffignac, r.G. Hill, Structural analysis of a series of strontium-substituted apatites, Acta biomaterialia, 4, 1455-1464 (2008).
75. J. Zeglinski, M. Nolan, M. Bredol, A. Schatte, S.A.M., Tofail, Unravelling the specific site preference in doping of calcium hydroxyapatite with strontium

from ab initio investigations and Rietveld analyses, RCS Physical Chemistry Chemical Physics, 14, 3435-3443 (2012).
76. S. Lala, M. Ghosh, P.K. Das, T. Kar, S.K. Pradhan, Magnesium substitution in carbonated hydroxyapatite: structural and microstructural characterization by Rietveld's refinement, Materials Chemistry and Physics, 170, 319-329 (2016).
77. A. El Yacoubi, A. Massit, S. El Moutaoikel, A. Rezzouk, B.C. El Idrissi, Rietveld refinement of the crystal structure of hydroxyapatite using x-ray powder diffraction, American Journal of Materials Science and Engineering, 5(1), 1-5 (2017).
78. Z.Y. Qiu, G. Li, Y.Q. Zhang, W. Hu, J. Ma, S.M. Zhang, Fine structure analysis and sintering properties of Si-doped hydroxyapatite, Biomedical materials, 045009 (2012).
79. R.T. Candidato Jr., R. Sergi, J. Jouin, O. Nogueira, L. Pawlowski, Advanced microstructural study of solution precursor plasma sprayed Zn doped hydroxyapatite coatings, Journal of the European Ceramic Society, 38, 2134-2144 (2018).
80. P.N. Kumar, S.K. Mishra, R.U. Kiran, S. Kannan, Preferential occupancy of strontium in the hydroxyapatite lattice in biphasic mixtures formed from non-stoichiometric calcium apatites, Dalton Transitions, 44, 8284-8292 (2015).
81. S. Gomes, G. Renaudin, A. Mesbah, E jallot, C. Bonhomme, F. Babonneau, J.-M. Nedelec, Thorough analysis of silicon substitution in biphasic calcium phosphate bioceramics: A multi-technique study, Acta Biomaterialia, 6(8), 3264-3274 (2010).
82. S. Gomes, J.-M. Nedelec, E. Jallot, D. Sheptyakov, G. Renaudin, Silicon location in silicate-substituted calcium phosphate ceramicsdetermined by neutron diffraction, Crystal Growth & Design, 11(90, 4017-4026 (2011).
83. V. Aina, G. Lusvardi, B. Annaz, I.R. Gibson, F.E. Imrie, G. malavasi, L. Menabue, G. Cerrato, G. Martra, magnesium- and strontium-co-substituted hydroxyapatite: the effects ofdopped-ions on the structure and chemico-physical properties, Journal of Materials Science: Materials in Medicine, 23, 2867-2879 (2012).
84. S. Kannan, F. Goetz-Neunhoeffer, J. Neubauer, A.H.S. Rebelo, P. Valerio, J.M.F. Ferreira, Rietveld structure and in vitro analysis on the influence of magnesium in biphasis (hydroxyapatite and β-tricalcium phosphates), Journal of Biomedical Materials Research Part B: Applied Biomaterials, 90B(1), 404-411 (2009).
85. M. Pereira Moreira, G.D. de Almeida Soares, J. Dentzer, k. Anselme, LA. De sena, A. Kuznetsov, E. Araujo dos Santos, Synthesis of magnesium- and manganese-doped hydroxyapatite structures assisted by the simultaneous incorporation of strontium, materials Science and Engineering C, 61, 736-743 (2016).
86. G. Cheng, Y. Zhang, Handi Yin, Y. Ruan, Y. Sun, K. Lin, Effects of strontium substitution on the structural distortion of hydroxyapatite by rietveld

refinement and Raman spectroscopy, Ceramics International, 45, 11073-11078 (2019).
87. K.A.S. Farias, W.J.B. Sousa, M.J.B. Cardoso, R.J.S. Lima, M.A. Rodriguez, M.V.L. Fook, Obtaining hydroxyapatite with different precursors for application as a biomaterial, Ceramica, 65, 99-106 (2019).
88. L. Wei, H. Yang, J. Hong, Z. He, C. deng, Synthesis and structure properties of se and Sr co-doped hydroxyapatite and their biocompatibility, Journal of Materials Science, 54, 2514-2525 (2019).
89. J.R. Guerra-Lopez, G.A. Echeverria, J.A. Guida, R. Vina, G. Punte, Synthetic hydroxyapatites doped with Zn(II) studied by X-ray diffraction, infrared, Raman and thermal analysis, Journal of Physics and Chemistry of Solids, 81, 57-65 (2015).
90. J. Zhao, J. Zhao, J.H. Chen, X.H. Wang, Z. Han, Y. Li, Rietveld refinement of hydroxyapatite, tricalcium phosphate and biphasicmaterials prepared by solution combustion method, Ceramics International, 3379-3388 (2014).
91. E.L. Moreira, J.C. Araujo, V.C.A. Moraes, A.P.D. Moreira, Analysis of a carbonated hydroxyapatite by X ray difraction using the Rietveld method, revista materia, 12(3), 494-502 (2007).
92. L. Guo, M. Huang, X. Zhang, Effects of sintering temperature on structure of hydroxyapatite studied with Rietveld method, Journal of Materials Science: Materials in medicine, 14, 817-822 (2003).
93. J.A. Rincon-Lopez, J.A. Hermann-Munoz, A.L. Giraldo-Betancur, A. De Vizcaya-Ruiz, J.M. Alvarado-Orozco, J. Munoz-Saldana, Synthesis, Characterization and in vitro study of synthetic and bovine-derived hydroxyapatite ceramics: a comparison, Materials, 11, 333, 1-17 (2018).
94. C. Meneghini, M.C. Dalconi, S. Nuzzo, S. Mobilio, R.H. Wenk, Rietveld refinement on x-ray diffraction patterns of bioapatite in human fetal bones, Biophysical journal, 84, 2021-2019 (2003).
95. N. Dobelin, Interlaboratory study on the quantification of calcium phosphates phases by Rietveld refinement, Powder diffraction, 30(3), 231-241 (2015).
96. M. Safarzadeh, S. Ramesh, C.Y. Tan, H. Chandran, Y.C. Ching, A.F. Mohd Noor, S. Krishnasamy, W. D. Teng, Sintering behaviour of carbonated hydroxyapatite prepared at different carbonate and phosphate ratios, Boletin de la Sociedad Española de Ceramica y Vidrio, 59, 73-80 (2020).
97. G. renaudin, P. Laquerriere, Y. Filinchuk, E. Jallot, J.M. Nedelec, Structural characterization of sol-gel derived Sr-substituted calcium phosphates with anti-osteoporotic and anti-inflammatory properties, Journal of Materials chemistry, 18, 3593-3600 (2008).
98. R.K. Brundavanam, G.E.J. Poinern, D. Fawcett, Modelling the crystal structure of a 30 nm sized particle based hydroxyapatite powder synthesized under the influence of ultrasound irradiation from x-ray powder diffraction data, American Journal of Materials Science, 3(4), 84-90 (2013).
99. D. Haverty, S.A.M. Tofail, K.T. Stanton, J.B. McMonagle, Structure and stability of hydroxyapatite: density functional calculation and rietveld analysis, Physical review B, 71, 094103 (2005).

100. D. J. Indrani, B. Soegijono, W.A. Adi, N. trout, Phase composition and crystallinity of hydroxyapatite with various heat treatment, International Journal of Applied Pharmaceutics, 9(2), 1-5 (2017).
101. M. Mir, F. Lima Leite, P.S. de Paula Herrmann Junior, F.L. Pisetti, A. Malta Rosii, E. Lima Moreira, Y. Primerano Mascarenhas, XRD, AFM, IR and TGA study on nanostructured hydroxyapatite, Materials research, 15(4), 622-627 (2012).
102. Y.M.Z. Ahmed, S.M. El-Sheikh, Zaki Z.I., Changes in hydroxyapatite powder properties via heat treatmet, Bulletin of Materials Science, 38, 1807-1819 (2015).
103. A.S.F. Alqap, I. Spopyan, Low temperature hydrothermal synthesis of calcium phosphate ceramics: effect of excess Ca precursor on phase behaviour, Indian Journal of Chemistry, 48A, 1492-1500 (2009).
104. S. Meejoo, W. Maneeprakorn, P. Winotai, Phase and thermal stability of nanocrystalline hydroxyapatite prepared via microwave heating. Thermochimica Acta, 447, 115–120 (2006).
105. J-K. Han, H-Y. Song, F. Saito, B.-Y. Lee, Synthesis of height purity nano-sized hydroxyapatite powder by microwave-hydrothermal method. Materials Chemistry and Physics, 99, 235 – 239 (2006).
106. M. Vukomanović, I. Bračko, I. Poljanšek, D. Uskokovič, S.D. Škapin, D. Suvorov, The Growth of Silver Nanoparticles and Their Combination with Hydroxyapatite To Form Composites via a Sonochemical Approach, Crystal Growth & Design, , 11(9), 3802-3812 (2011).
107. L. Yang, X. Ning, Q. Xiao, K. Chen, H. Zhou, Development and characterization of porous silver-incorporated hydroxyapatite ceramic for separation and elimination of microorganisms, Journal of Biomedical Materials Research, Part B: Applied Biomaterials, , 81B, 50-56 (2007).
108. X. Bai, K. More, M.C. Rouleau, A. Rabiei, Functionally graded hydroxyapatite coatings doped with antibacterial components, Acta Biomaterialia, 6(6), 2264 -2273 (2010).
109. V. Stanic, D. Janackovic, S. Dimitrijevic, B.S. Tanaskovic, M. Mitric, S.M. Pavlovic, A. Krstic, D. Jovanovic, S. Raicevic, Synthesis of antimicrobial monophase silver-doped hydroxyapatite nanopowders for bone tissue engineering, Applied Surface Science, 257, 4510-4518 (2011).
110. P.N. Lim, L. Chang, E.S. Thian, Development of nanosized silver-substituted apatite for biomedical applications: A review, Nanomedicine, 11(6), 1331-1344 (2015).
111. W.K. Jung, H.C. Koo, K.W. Kim, S. Shin, S.H. Kim, Y.H. Park, Antibacterial activity and mechanism of action of the silver ion in Staphylococcus aureus and Escherichia coli, Applied and Environmental Microbiology, 74, 2171-2178 (2008).
112. Q.L. Feng, J. Wu, G.Q. Chen, F.Z. Cui, T.N. Kim, J.O. Kim, A mechanistic study of the antibacterial effect of silver ions on Escherichia coli and Staphylococcus aureus, Journal of Biomedical Materials Research, 52(4), 662-668 (2000).

113. I. Chopra, The increasing use of silver-based products as antimicrobial agents: a useful development or a cause for concern?, Journal of Antimicrobial Chemotherapy, 59(4), 587590 (2007).
114. S.H. Kim, H.S. Lee, D.S. Ryu, S.J. Choi, D.S. Lee, Antibacterial Activity of Silver-nanoparticles Against Staphylococcus aureus and Escherichia coli, Korean Journal of Microbiology and Biotechnology, 39(1), 77-85 (2011).
115. A.R. Shahverdi, A. Fakhimi, H.R. Shahverdi, S.Minaian. Synthesis and effect of silver nanoparticles on the antibacterial activity of different antibiotics against Staphylococcus aureus and Escherichia coli, Nanomedicine: Nanotechnology, Biology, and Medicine, 3(2), 168171 (2007).
116. A.M. Fayaz, K. Balaji, M. Girilal, R. Yadav, P.T. Kalaichelvan, R. Venketesan, Biogenic synthesis of silver nanoparticles and their synergistic effect with antibiotics: a study against gram-positive and gram-negative bacteria, Nanomedicine: Nanotechnology, Biology, and Medicine, 6(1), 103-107 (2010).
117. W. Suvannapruk, F. Thammarakcharoen, P. Phanpiriya, J. Suwanprateeb, development of antibiotics impregnated nanosized silver phoasphate-doped hydroxyapatite bone graft, Journal of Nanomaterials, 542584, 1-9 (2013).
118. . J.R. Morones-Ramirez, J.A. Winkler, C.S. Spina, J.J. Collins, Silver enhances antibiotic activity against gram-negative bacteria, Science Translational Medicine, 5(190), 190ra81 (2013). DOI: 10.1126/scitranslmed.3006276
119. V.G. Voronin, I.D. Petrova, A.N. Leksin, B.V. Shemeryankin, Pharmaceutical Chemistry Journal, 10(9), 1215-1217 (1976).
120. A. Sobke, M. Klinger, B. Hermann, S. Sachse, S. Nietzsche, O. Makarewicz, P.M. Keller, W. Pfister, E. Straube, The urinary antibiotic 5-nityro-8-hydroxyquinoline (nitroxoline) reduces the formation and induces the dispersal of Pseudomonas aeruginosa biofilms by chelation of iron and zinc, Antimicrobial Agents and Chemotherapy, 56(11), 6021-6025 (2012).
121. Y. Cong, J. Wang, C. Du, S. Han, L. Meng, H. Zhao, Solubility determination and thermodynamic modeling of 5-nitro-8-hydroxyquinoline in ten organic solvents from T = (278.15 to 313.15) K and mixing properties of solutions,The Journal of Chemical Thermodynamics, 100, 60-71 (2016).
122. Gh. Tomoaia, A. Mocanu, L.-D. Bobos, L.-B. Pop, O. Horovitz, M. Tomoaia-Cotisel, Biocomposites for orthopedic applications, Studia UBB Chemia, 60(3), 265-272 (2015).
123. Gh. Tomoaia, M. Tomoaia-Cotisel, L. B. Pop, A. Pop, O. Horovitz, A. Mocanu, N. Jumate, L.-D. Bobos, Surface potentials of cholesterol and dimyristoyl phosphatidylcholine monolayers at the air/water interface, Revue Roumaine de Chimie, 56(10-11), 1039-1046 (2011).
124. Gh. Tomoaia, L.B. Pop, I. Petean, M. Tomoaia-Cotisel, Significance of surface structure on orthopedic materials, Materiale Plastice, 49(1), 48-54 (2012).
125. X. Wei, M. Luo, H. Liu, Preparation of the antithrombotic and antimicrobial coating through layer-by-layer self-assembly of nattokinase-nanosilver complex and polyethylenimine, Colloids and Surfaces B: Biointerfaces, 116(1), 418-423 (2014).

126. B. Zhou, Y. Li, H. Deng, Y. Hu, B. Li, Antibacterial multilayer films fabricated by layer-by-layer immobilizing lysozyme and gold nanoparticles on nanofibers, Colloids and Surfaces B: Biointerfaces, 116(1), 432-438 (2014).
127. L.H. Silva Almeida, R.R. Moraes, R.D. Morgental, F.G. Pappen, Are premixed calcium silicate-based endodontic sealers comparable to conventional materials? A systematic review of in vitro studies, Journal of Endodontics, 43(4), 527-535 (2017).
128. G. Debelian, M. Trope, The use of premixed bioceramic materials in endodontics, Giornale Italiano di Endodonzia, 30(2), 70-80 (2016).
129. P. Bali, A.K. Shivekshith, C.R. Allamaprabhu, H.P. Vivek, Calcium enriched mixture cement: a review, International Journal of Contemporary Dental and Medical Reviews, 061214, 1-3 (2014).
130. F. Panahi, S.M. Rabiee, R. Shidpour, Synergic effect of chitosan and dicalcium phosphate on tricalcium silicate-based nanocomposite for root-end dental application, Materials Science and Enginneering C, 80(1), 631-641 (2017).
131. I.R. Oliveira, T.L. Andrade, K.C.M.L. Araujo, A.P. Luz, V.C. Pandolfelli, Hydroxyapatite synthesis and the benefits of its blend with calcium aluminate cement, Ceramics International, 42, 2542-2549 (2016).
132. F. Goga, E. Forisz, A. Avram, A. Rotaru, A. Lucian, I. Petean, A. Mocanu, M. Tomoaia-Cotisel, Synthesis and thermal treatment of hydroxyapatite doped with magnesium, zinc and silicon, Revista de Chimie (Bucharest), 68(6), 1193-1200 (2017).
133. J.A. Lett, M. Sundareswari, K. Ravichandran, Porous hydroxyapatite scaffolds for orthopedic and dental applications - the role of binders, Materials Today: Proceedings, 3(6), 1672-1677 (2016).
134. S.M. Rabiee, F. Moztarzadeh, M. Solati-Hashjin, Synthesis and characterization of hydroxyapatite cement, Journal of Molecular Structure, 969(1-3), 172-175 (2010).
135. M. Hosseinzade, R.K. Soflou, A. Valian, H. Nojehdehian, Physicochemical properties of MTA, CEM, hydroxyapatite and nano Hydroxyapatite-chitosan dental cements, Biomedical Research, 27(2), 442 (2016).
136. Y.A. Moreno-Vargas. J.P. Luna-Arias, J.O. Flores-Flores, E. Orozco, L. Bucio, Hydration reactions and physicochemical properties in a novel tricalcium-dicalcium silicate-based cement containing hydroxyapatite nanoparticles and calcite: A comparative study, Ceramics International, 43(16), 13290-13298 (2017).
137. J. Camilleri, F.E. Montesin, R.V. Curtis, T.R. Pitt Ford, Characterization of Portland cement for use as a dental restorative material, Dental Materials, 22(6), 569-575 (2006).
138. V. Bortolotti, P. Fantazzini, R. Mongiorgi, S. Sauro, S. Zanna, Hydration kinetics of cements by time-domain nuclear magnetic resonance: application to portand-cement-derived endodontic pastes, Cement and Concrete Research, 42(3), 577-582 (2012).
139. W.N. Ha, D.P. Bentz, B. Kabler, L.J. Walsh, D90: the strongest contributor to setting time in mineral trioxide aggregate and Portland cement, Journal of Endodontics, 41(7), 1146-1150 (2015).

140. A.M. Negm, E.E. Hassanien, A.M. Abu-Seida, M.M. Nagy, Biological evaluation of a new pulp capping material developed from Portland cement, Experimental and Toxicologic Pathology, 69(3), 115-122 (2017).
141. M.G. Gandolfi, P. Taddei, A. Tinti, E. De Stefano Dorigo, C. Prati, Alpha-TCP improves the apatite-formation ability of calcium-silicate hydraulic cement soaked in phosphate solution, Materials Science and Engineering C, 31(7), 1412-1422 (2011).
142. N.J. Coleman, J.W. Nicholson, K. Awosanya, A preliminary investigation of the in vitro bioactivity of white Portland cement, Cement and Concrete Research, 37(11), 1518-1523 (2007).
143. D. Araki Ribeiro, M.A. Hungaro Duarte, M. Akemi Matsumoto, M.E. Alencar Marques, D.M. Favero Salvadori, Bioompatibility in vitro tests of mineral trioxide aggregate and regular and white Portland cements, Journal of Endodontics, 31(8), 605-607 (2005).
144. A. Chaipanich, P. Torkittikul, Microstructure: surface and cross-sectional studies of hydroxyapatite formation on the surface of white Portland cement paste in vitro, Applied Surface Science, 257(20), 8385-8390 (2011).
145. J. Camilleri, Characterization and hydration kinetics of tricalcium silicate cement for use as a dental biomaterial, Dental Materials, 27(8), 836-844 (2011).
146. P. Scembri-Wismayer, J. Camilleri, Why biphasic? Assesment of the effect on cell proliferation and expression, Journal of Endodontics, 43(5), 751-759 (2017).
147. N. Wongkornchaowalit, V. Lertchirakarn, Setting time and flowability of accelerated Portalnd cement mixed with polycarboxylate superplasticizer, Journal of Endodontics, 37(3), 387-389 (2011).
148. P. Torkittikul, A. Chaipanich, Optimization of calcium chloride content on bioactivity and mechanical properties of white Portland cement, Materials Science and Engineering C, 32(2), 282-289 (2012).
149. K.B. Wiltbank, S.A. Schwartz, W.G. Schindler, Effect of selected accelerants on the physical properties of mineral trioxide aggregate and Portland cement, Journal of Endodontics, 33(10), 1235-1238 (2017).
150. L. Wang, X. Xie, C. Li, H. Liu, K. Zhang, Y. Zhou, X. Chang, H.H.K. Xu., Novel bioactive root canal sealer to inhibit endodontic multispecies biofilms with remineralizing calcium phosphate ions, Journal of Dentistry, 60, 25-35 (2017).
151. R.D. Pasca, G. Tomoaia, A. Mocanu, I. Petean, G.A. Paltinean, O. Soritau, M. Tomoaia-Cotisel, Porous collagen scaffolds for bone regeneration, Studia UBB Chemia, 60(3), 257-264 (2015).
152. M.A. Naghiu, M. Gorea, E. Mutch, F. Kristaly, M. Tomoaia-Cotisel, Forsterite nanopowder: structural characterization and biocompatibility evaluation, Journal of Material Science and Technology, 29(7), 628-232 (2013).
153. Gh. Tomoaia, O. Horovitz, A. Mocanu, A. Nita, A. Avram, C.P. Racz, O. Soritau, M. Cenariu, M. Tomoaia-Cotisel, Effects of doxorubicin mediated by gold nanoparticles and resveratrol in two human cervical tumor cell lines, Colloids and Surfaces B: Biointerfaces, 135, 726-734 (2015).

154. M. Tomoaia-Cotisel, A. Tomoaia-Cotisel, T. Yupsanis, G. Tomoaia, I. Balea, A. Mocanu, Cs. Racz, Coating layers of major storage protein from aleurone cells of barley by atomic force microscopy, Revue Roumaine de Chimie, 51(12), 1181-1185 (2006).
155. P.T. Frangopol. D.A. Cadenhead, G. Tomoaia, A. Mocanu, M. Tomoaia-Cotisel, The effect of procaine on lipid domains investigated by contact mode atomic force microscopy, Revue Roumaine de Chimie, 60(2-3), 265-273.
156. F. Tavangarian, R. Emadi, Nanostructure effects on the bioactivity of forsterite bioceramic, Materials letters, 65(4), 740–743 92011).
157. S. Oh, N. Oh; M. Appleford, J.L. On, American Journal of Biochemistry & Biotechnology, 2(2), 49–56 (2006).
158. S. Ni, L. Chou, J. Chang, Preparation and characterization of forsterite (Mg_2SiO_4) bioceramics, Ceramics International, 33(1), 83–88 (2008).
159. K.Y.S. Lee, K.M.C. Chin, S. Ramesh;,J. Purbolaksono, M.A., Hassan, M. Hamdi, W. D. Teng, Characterization of forsterite ceramics, Journal of Ceramic Processing Research,14(1), 131-133 (2013).
160. M. Kharaziha, M.H. Fathi, Improvement of mechanical properties and biocompatibility of forsterite bioceramic addressed to bone tissue engineering materials, Journal of the Mechanical Behavior of Biomedical Materials, 3(7), 530–537 (2010).
161. M. Saqaei, M. Fathi; H. Edris, V. Mortazavi, N. Hosseini, Effects of adding forsterite bioceramic on in vitro activity and antibacterial properties of bioactive glass-forsterite nanocomposite powders, Advanced Powder Technology, 27(5), 1922-1932 (2016).
162. A. Krajewski, A. Ravaglioli, E. Roncari, P. Pinasco, L. Montanari, Porous ceramic bodies for drug delivery, Jjournal of Materials Science: Materials in Medicine, 11(12), 763–771 (2000).
163. M. Saqaei, M. Fathi, H. Edris, V. Mortazavi, Preparation and biocompatibility evaluation of bioactive glass–forsterite nanocomposite powder for oral bone defects treatment applications, Materials Science and Engineering C 56, 409-416 (2015).
164. G. Furtos, M.A. Naghiu, H. Declercq, M. Gorea, C. Prejmerean, O. Pana, M. Tomoaia-Cotisel, Nano forsterite biocomposites for medical applications: Mechanical properties and bioactivity, Journal of Biomedical Materials Research Part B: Applied Biomaterials, 104(7), 1290-1301 (2015).
165. S. Naghieh, E. Foroozmehr, M. Badrossamay, M. Kharaziha, Combinational processing of 3D printing and electrospinning of hierarchical poly(lactic acid)/gelatin-forsterite scaffolds as a biocomposite: Mechanical and biological assessment, Materials & Design 133, 128-135 (2017).
166. R. Choudhary, P. Manohar, J. Vecstaudza, M .J. Yáñez-Gascón, H. Pérez Sánchez,R. Nachimuthu, J. Locs, S. Swamiappan, Preparation of nanocrystalline forsterite by combustion of different fuels and their comparative in-vitro bioactivity, dissolution behaviour and antibacterial studies, Materials Science and Engineering C, 77, 811-822 (2017).

167. M. Zabihi, M.R. Ayatollahi, H.R.Rezaie, Mixed-mode fracture of synthesized nanocrystalline forsterite for biomedical applications, Theoretical and Applied Fracture Mechanics, 94, 173-180 (2018).
168. H. Ghomi, M. Jaberzadeh, M.H. Fathi, Novel fabrication of forsterite scaffold with improved mechanical properties, Journal of Alloys and Compounds, 509(5), L63-L68 (2011).
169. S.M. Mirhadi, A. Forghani,F. Tavangarian, A modified method to synthesize single-phase forsterite nanoparticles at low temperature, Ceramics International, 42(7), 7974-7979 (2016).
170. M.A. Naghiu, M. Gorea, F. Kristaly, M. Tomoaia-Cotisel, A new method for synthesis of forsterite nanomaterials for bioimplants, Ceramics-Silikaty, 58(4), 303-307 (2014).
171. M. Gorea, M.A. Naghiu, M. Tomoaia-Cotisel, G. Borodi, Nano and microstrucure effects on the bioactivity of forsterite powders, Ceramics-Silikaty, 57(2), 87-91 (2013).
172. Y. Xie, W. Zhai, L. Chen, J. Chang, X. Zheng, C. Ding, Preparation and in vitro evaluation of plasma-sprayed Mg_2SiO_4 coating on titanium alloy, Acta Biomaterialia, 5(6), 2331-2337 (2009).
173. R. Choudhary, A. Chatterjee, S K. Venkatraman, S. Koppala, J. Abraham, S. Swamiappan, Antibacterial forsterite (Mg_2SiO_4) scaffold: A promising bioceramic for load bearing applications., Bioactive Materials, 3(3), 218-224 (2018).
174. A. Danistean, M. Gorea, A. Avram, S. Rapuntean, Gh. Tomoaia, A. Mocanu, C. Garbo, O. Horovitz, M. Tomoaia-Cotisel, Antimicrobial activity of ceramic disks loaded with silver ions and nitroxoline, Studia UBB Chemia, 61(3), 275-283 (2016).
175. U.V. Zdrenghea, Gh. Tomoaia, D.-V. Pop-Toader, A. Mocanu, O. Horovitz, M. Tomoaia-CotiselProcaine effect on human erythrocyte membrane explored by atomic force microscopy, Combinatorial Chemistry & High Throughput Screening, 14(4), 237-247 (2011).
176. D. Dufrane, C. Delloye, I.J. Mckay, P.N. De Aza, S. De Aza, Y.J. Schneider, M. Anseau, Indirect cytotoxicity evaluation of pseudowollastonite, Journal of Materials Science: Materials in Medicine, 14(1), 33–38 (2003).
177. J. Y. Rho, R. B. Ashman, C. H. Turner, Young's modulus of trabecular and cortical bone material: Ultrasonic and microtensile measurements, Journal of Biomechanics, 26(2),111-119 (1993).
178. D. Li, S. Liu, Water Quality Monitoring and Management – Basis, Technology and Case Study, Academic Press, chapter 10 (2019).
179. S. Suthar, V. Chhimpa, S. Singh, Bacterial contamination in drinking water: a case study in rural areas of northern Rajasthan, India Environmental Monitoring and Assessment, 159,43–50, (2009).
180. World Health Organization, Guidelines for Drinking-water Quality – First Addendum to Third Edition, Volume 1: Recommendations, Third Edition.
181. G. Gabutti , A. de Donno, F. Bagordo, M. T., Montagna, Comparative survival of faecal and human contaminants and use of Staphylococcus aureus as an

effective indicator of human pollution, Marine Pollution Bulletin, 40(8), 697-700 (2000).
182. A.H.M. Batista, A.C.D. Moreira, R.M. de Carvalho, G.W.P. Sales, P.C.N. Nogueira, T.B.Grangeiro, S.C. Medeiros, E.R. Silveira, N.A.P. Nogueira, Anrimicrobial effects of violacein against Planktonic cells and biofilms of Staphylococcus aureus, Molecules, 22, 1543 (2017).
183. M.Z. David, R.S. Daum, Community-associated methicilin-resistant Staphylococcus aureus: epidemiology and clinical consequences of an emerging epidemic, Clinical Microbiology Reviews, 23(3), 616-687 (2010).
184. O.K. Ince, , M. Ince, N.M. Kraaslan, V. Yonten, Optimization of Cadmium Removal From Water by Hydroxyapatite Using Experimental Design Methodology, Analytical Letters, 49(15), 2513-2524 (2016).
185. S. Zamani, E. Salahi, I. Mobasherpour, Removal of Nickel from Aqueous Solution by Nano Hydroxyapatite Originated from Persian Gulf Corals, Canadian Chemical Transactions, 1(3), 173-190 (2013).
186. A. Costescu, E. Andronescu, B.S. Vasile, R. Trusca, P. Le Coustumer, E.S. Barna, S.L. Iconaru, M. Montelica-Heino, C.S. Ciobanu, Synthesis and characterization of dextran coated hydroxyapatite for environmental application, Scientific Bulletin-univeristy Politehnica of Bucharest Series B, 76(4), 71-80 (2014).
187. A. Corami, S. Mignardi, V. Ferrini, Cadmium removal from single- and multi-metal (Cd + Pb +Zn+ Cu) solutions by sorption on hydroxyapatite, Journal of Colloid and Interface Science, 317, 402-408 (2008).
188. D.T.M. Hieu, P.T.T. Tran, A.K. Ton, M.V. Le, , A Novel Method for the Fabrication of Granular Hydroxyapatite-bentonite Composite Adsorbents for the Removal of Pb2+ from an Aqueous Solution, Journal of Environmental Science and Engineering B, 5, 371-378 (2016).
189. M. Nehru, S. Sumathi, Removal of Cadmium (II) and Nickel (II) Ions by Copper Substituted Hydroxyapatite, International Journal of Applied Engineering Research, 8(19), 2179-2181 (2013).
190. F. Fernane, S. Boudia, H. Saouli, Interactions between calcium phosphate and heavy metal ions in aqueous solution, MATEC Web of Conferences, 5, 1-5 (2013).
191. Q.Y. Ma, S.J. Traina, T.J. Logan, I n Situ Lead Immobilization by Apatite, Environmental Science and Technology, 27, 1803-1810 (1993).

Chapter 15. ORIGINAL RESEARCH ACTIVITY RESULTS

15.1. ORIGINAL SCIENTIFIC PAPERS

10 articles were published in scientific journals listed ISI and one article in Procedings Volume II, Integral Communications Autumn Conference, Real

Convergence Romania-European Union, Academy of Scientists. The paper [1] was awarded by UEFISCDI (red zone). **Cumulative impact factor: 11.768.**

Google Scholar:
https://scholar.google.ro/citations?user=rVuN0gAAAAJ&hl=en

Total citations - 61
h-index 4

List of ISI published articles

1. Gh. Tomoaia, O. Horovitz, A. Mocanu, A. Nita, **A. Avram**, C. P. Racz, O. Soritau, M. Cenariu, M. Tomoaia-Cotisel, effects of doxorubicin mediated by gold nanoparticles and resveratrol in two human cervical tumor cell lines, Colloids and Surfaces B: Biointerfaces, 135, 726-734 (2015). **IF= 3.973**. **Citations - 36.**
2. F. Goga, E.Forizs, **A. Avram**, A. Rotaru, A. Lucian, I. Petean, A. Mocanu, M. Tomoaia-Cotisel, Synthesis and thermal treatment of hydroxyapatite doped with magnesium, zinc and silicon, Revista de Chimie (Bucuresti), 68(6), 1193-1200 (2017). **IF=1.605. Citations -10.**
3. F. Goga, E. Forizs, G. Borodi, G. Tomoaia, **A. Avram**, R. Balint, A. Mocanu, O. Horovitz, M. Tomoaia Cotisel, Behavior of doped hydroxyapatites during the heat treatment, Revista de Chimie (Bucuresti), 68(12), 2907-2913 (2017). **IF=1.605. Citations - 2.**
4. E. Forizs, F. Goga, **A. Avram**, A. Mocanu, I. Petean, O. Horovitz, M. Tomoaia-Cotisel, Thermal analysis of pure and multisubstituted hydroxyapatite pastes, Studia Universitatis Babes-Bolyai, Chemia 62(4), 2017, 173-180. **IF=0.275**.
5. A. Danistean, M. Gorea, **A. Avram**, S. Rapuntean, M.Aurora, G. Tomoaia, C. Garbo, O.Horovitz, M. Tomoaia-Cotisel, Antimicrobial activity of ceramic desks loaded with nitroxoline, Studia Universitatis Babes-Bolyai, Chemia, 61(3), 275-283 (2016). **IF=0.275**. **Citations - 3.**
6. **A. Avram**, M. Gorea, R. Balint, L. Timis, S. Jitaru, A. Mocanu, M. Tomoaia-Cotisel, Portland cement enriched with hydroxyapatite for endodontic applications, Studia Universitatis Babes-Bolyai, Chemia, 62(4), 81-92 (2017). **IF=0.275**.
7. M. Gorea, M.-A. Naghiu, **A. Avram**, I. Petean, M. Tomoaia-Cotisel, Sintering and characterization of some new forsterite ceramics, Studia Universitatis Babes-Bolyai, Chemia, 64(2), 383-392 (2019). **IF= 0.275**.
8. M. Gorea, M.-A. Naghiu, **A. Avram**, I. Petean, A. Mocanu, M. Tomoaia-Cotisel, Novel porous forsterite ceramics. Biocompatibility and bioactivity evaluation, Revista de Chimie (Bucuresti), 71(2), 343-351 (2020). IF= **1.605**. **Citations - 1.**
9. **A. Avram**, M. Gorea, S. Rapuntean, A. Mocanu, G. A. Paltinean, C. Varhelyi Jr., O. Horrovitz, M. Tomoaia-Cotisel, In-vitro antibacterial activity of novel nanostructured composites based on forsterite and silver nanoparticles,

Revista de Chimie (Bucuresti), 71(1), 13-21 (2020). IF= **1.605**. **Citations - 1.**

10. **A. Avram**, T. Frentiu, O. Horovitz, A. Mocanu, F. Goga, M. Tomoaia-Cotisel, Hydroxyapatite for removal of heavy metals from wastewater, Studia Universitatis Babes-Bolyai, Chemia, 62(4), 93-104 (2017). IF=**0.275**. **Citations - 8.**

List of articles published in Proceedings

1. **A. Avram**, M. Gorea, A. Mocanu, M. Tomoaia-Cotisel, Cercetarea și dezvoltarea unor compozite formate din forsterit, colagen și PLA depuse pe implanturi metalice, Academia Oamenilor de Știință, Conferinta de Toamnă, Convergența Reala Romania-Uniunea Europeană, Volumul II, Comunicari Integrale, Brasov 20-21 Septembrie, 258-265 (2019), ISBN 978-973-618-430-7. IF=0.

15.2. Participation in conferences and symposia

The scientific results were presented in 7 conferences obtaining an award for „**the best poster"** at the conference [5].

List of conferences

1. **A. Avram**, F. Goga, M. Tomoaia - Cotisel, Zeolite type A - preparation, characterization and further applications, 6th International Conference Biomaterials, Tissue Engineering and Medical Devices (BiomMedD'2014), Constanta Romania September 17-20, (2014).
2. **A. Avram**, F. Goga, A. Mocanu, M. Tomoaia - Cotisel, Hydroxyapatite biomimetic ceramic synthesized by a novel sol-gel method, COST Action NP1301 New Generation Biomimetic and Customized Implants for Bone Engineering. Biomaterials for Dental and Orthopedic Applications, Cluj-Napoca, Romania March 13-15, (2017).
3. **A. Avram**, M. Gorea, N. Har, A. Mocanu, M. Tomoaia-Cotişel, Porous forsterite 3D scaffolds with potential osseo-regenerative properties - a preliminary study, The 11th Edittion of the Symposium with International Participation Dedicated to the Romania's Great Union Centenary New Trends and Strategiesi The Chemistry of Advanced Materials with Relevance in Biological Systems, Technique and Environmental Protection, Timişoara, România June 28-29, (2018).
4. L. Timis, **A. Avram**, M. Gorea, I. Bota, I. Petean, M. Tomoaia-Cotişel, Synthesis and characterization of tricalcium silicate as a main component of endodontic cement, The 11th Edittion of the Symposium with International Participation Dedicated to the Romania's Great Union Centenary New Trends and Strategiesi The Chemistry of Advanced Materials with Relevance in Biological Systems, Technique and Environmental Protection, Timişoara, România June 28-29, (2018).

5. **A. Avram**, A. M. Naghiu, M. Gorea, Maria Tomoaia-Cotişel, Forsterite porous nanoceramics as a novelty in medical applications, International Conference on Materials Science & Materials Chemistry, Paris, France, 20- 22 August, (2018),
6. **A. Avram**, M. Gorea, A. Mocanu, M. Tomoaia-Cotisel, Cercetarea si dezvoltarea unor Compozite Formate din Forsterit, Colagen si PLA depuse pe Implanturi Metalice, September, Conferinta nationala Stiintifica, Acasemia oamenilor de Stiinta din Romania 20-21 Septembrie 2019 Brasov, Volum de Rezumate, 13(2), 79 (2019).
7. **A. Avram**, M. Gorea, A. Mocanu, M. Tomoaia-Cotisel, The influence of synthesis methods on the characteristics of porous forsterite ceramics, 12th International Conference Processes in Isotopes and Molecules Cluj-Napoca 25-26 September 86 (2019).

15.3. Activity in reasearch grants

The doctoral student has worked as a research assistant in 5 scientific research projects carried out in the Center for Scientific Research in Physical Chemistry, CECHIF, under the supervision of Univ. Prof. Dr. Maria Tomoaia-Cotişel, at Faculty of Chemistry and Chemical Engineering, FCIC, Babeş-Bolyai University of Cluj-Napoca, UBB.

List of scientific grants

1. IDEI grant 257/ 2011- 2014

Multifunctional nanostructures formed of gold or silver nanoparticles and different biomolecules with medical applications, **NANOMED.**

2. PN2 Partnership grant 171/ 2012 -2015

Development of new tools and smart composites based on advanced nanotehnology for medical applications, **DONTAS.**

3. EuroNanoMed grant nr. 4005/2013 2014-2017

Multifunctional injectable nano HAP composites for the treatment of osteoporotic bone fractures, **NanoForOsteo.**

4. PN2 Partnership grant 241 / 2014 -2016

Development of innovative nanomaterials based on advanced nanotechnology with applicability in prophylaxis of dental and periodontal diseases**, InovaMat.**

5. PCE grant 83 / 2017 -2019

Innovative composites with antimicrobial properties comprising ceramic nanoparticles and silver nanoparticles, functionalized with biomolecules, embedded into polymer matrix, **NanoSilva.**

15.4. Member in the Center of Scientific Research in Physical Chemistry

The doctoral student is a member of the Center of Scientific Research in Physical Chemistry, CECHIF, led by the Director, Univ. Prof. Dr. Maria Tomoaia-Cotișel, at Faculty of Chemistry and Chemical Engineering, FCIC, from Babeș-Bolyai University of Cluj-Napoca, UBB.